ELSEVIER

Journal of Hazardous Materials 45 (1996) 107–139

JOURNAL OF HAZARDOUS MATERIALS

Uncertainty and sensitivity analysis for gas and brine migration at the Waste Isolation Pilot Plant: Permeable shaft with panel seals

J.C. Helton[a,*], J.E. Bean[b], B.M. Butcher[c], J.W. Garner[d], J.D. Schreiber[e], P.N. Swift[c], P. Vaughn[c]

[a] *Department of Mathematics, Arizona State University, Tempe, AZ 85287, USA*
[b] *New Mexico Engineering Research Institue, Albuquerque, NM 87106, USA*
[c] *WIPP Performance Assessment Department 6342, Sandia National Laboratories, Albuquerque, NM 87185-1328, USA*
[d] *Applied Physics, Inc., Albuquerque, NM 87109, USA*
[e] *Science Applications International Corp., Albuquerque, NM 87106, USA*

Received 3 July 1994; accepted 5 May 1995

Abstract

Uncertainty and sensitivity analysis techniques based on Latin hypercube sampling, partial correlation analysis, stepwise regression analysis and examination of scatter plots are used in conjunction with the BRAGFLO model to examine two-phase (i.e., gas and brine) flow at the Waste Isolation Pilot Plant (WIPP), which is being developed by the US Department of Energy as a disposal facility for transuranic waste. The following topics are investigated to develop insights on factors that are potentially important in establishing compliance with applicable regulations of the US Environmental Protection Agency (i.e., 40 CFR 191, Subpart B; 40 CFR 268): (1) gas production due to corrosion of steel; (2) gas production due to microbial degradation of cellulosics; and (3) gas migration through a sealed shaft to the Culebra Dolomite. Important variables identified in the analysis include initial brine saturation of the waste, stoichiometric terms for corrosion of steel and microbial degradation of cellulosics, and seal permeabilities.

Keywords: Brine migration; Gas migration; Sensitivity analysis; Uncertainty analysis; Waste Isolation Pilot Plant

1. Introduction

The Waste Isolation Pilot Plant (WIPP) in southeastern New Mexico is being developed by the US Department of Energy (DOE) as a research and development

* Corresponding author.

SSDI 0304-3894(95)00082-8

facility to demonstrate the safe disposal of defense-generated transuranic waste [1–3]. The WIPP must comply with various environmental regulations of the US Environmental Protection Agency (EPA), including 40 CFR 268.6, *Petitions to Allow Land Disposal of a Waste Prohibited under Subpart C of Part* 268, which implements the Resource Conservation and Recovery Act (RCRA), [4] and 40 CFR 191, Subpart B, *Environmental Standards for the Management and Disposal of Spent Nuclear Fuel, High-Level and Transuranic Radioactive Wastes* [5]. In support of the development of the WIPP and to provide perspective on compliance with various applicable regulations, Sandia National Laboratories (SNL) is conducting an ongoing performance assessment (PA) for the WIPP [6, 7]. As part of this project, a sequence of annual PAs has been carried to summarize what is known about the WIPP and to provide guidance for future work [8–11].

The 1991 WIPP PA [10, 12–16] is the first to model the generation of gas in the repository and the potential flow of this gas away from the repository. The primary focus of prior PAs for the WIPP has been on compliance with 40 CFR 191, Subpart B, which primarily involves radionuclide releases due to cuttings removal and transport by groundwater. The two-phase (i.e., gas and brine) flow calculations performed for the 1991 WIPP PA provide the first opportunity to investigate factors that may influence compliance with 40 CFR 268.6.

To provide perspective on factors influencing compliance with 40 CFR 268, three analysis cases were considered in the 1991 WIPP PA: fully consolidated shaft (Case 1), system of shaft seals with panel seals (Case 2), and single shaft seal without panel seals (Case 3) [17, 18]. All three cases involve the undisturbed performance of the WIPP over 10 000 yr. Case 1 uses a model configuration identical to that used in the 1991 WIPP PA for scenarios involving human intrusion due to exploratory drilling for natural resources, with the significant difference that an intrusion does not occur. Because the Case 1 model configuration was designed to assess flow up a borehole, shafts are, depending on preferred terminology, omitted or assumed to be consolidated fully. This assumption forces all significant fluid flow from the repository to occur horizontally through anhydrite layers above and below the waste panels. Cases 2 and 3 contain permeable shafts, with the result that both horizontal and vertical fluid migration is possible.

For each case, uncertainty and sensitivity analyses are performed to determine the factors affecting gas and brine movement away from the repository. Gas movement provides an indication of the extent to which volatile organic compounds (VOCs) might be transported away from the repository. Similarly, brine movement provides an indication of the extent to which heavy metals and other contaminants might be transported away from the repository by flowing brine. The uncertainty and sensitivity analyses use techniques based on Latin hypercube sampling, examination of scatter plots, partial correlation analysis and stepwise regression analysis [19, 20].

The present paper presents results obtained in the analysis for a system of shaft seals with panel seals (i.e., Case 2). The results for Cases 1 and 3 are presented elsewhere [21, 22].

2. Summary description

Unlike the single isolated waste panel of Case 1 [21], the entire repository is modeled in the present analysis. Further, the present analysis explicitly incorporates the repository shafts and uses a more detailed characterization of the waste and its surroundings by representing the repository as a sequence of waste, panel seal, backfill and shaft regions through which gas and brine flow can occur in both the vertical and horizontal directions.

As shown in Fig. 1, the computational implementation of the analysis with the BRAGFLO model for two-phase flow [12, Section 5.2, Appendix A; 16, Section 3.1; 21, Section 3] is based on a rectangular grid aligned north-south through the repository. This grid is a simplification of the three-dimensional structure of the repository and involves several assumptions. The storage regions (i.e., waste panels) of the repository are grouped into the following three blocks on the basis of the number of drift and panel seals between the waste and the nearest shaft: Waste Block A, which corresponds to the single waste panel that is separated from the waste and exhaust shafts by two sets of panel seals (i.e., the Northern Panel in Fig. 2), Waste Block B, which corresponds to the five waste panels separated from the waste and exhaust shafts by three sets of panel seals (i.e., Panels 1, 2, 7 and 8 and the Southern Panel in Fig. 2), and Waste Block C, which corresponds to the four waste panels separated from the waste and exhaust shafts by four sets of panel seals (i.e., Panels 3, 4, 5 and 6 in Fig. 2). Each waste block contains the storage volume of the corresponding waste panels and drifts. The four shafts are combined into a single shaft at the location of the waste shaft, which is the shaft nearest the waste-disposal panels (Fig. 2), and this single shaft is subdivided vertically into four segments. Stratigraphic layers are assumed to be parallel and horizontal. The marker beds within the Salado Formation are actually slightly undulatory, with a drop of less than 1° to the southeast at the WIPP. Because the repository is being excavated at a constant stratigraphic horizon rather than at a constant elevation, this dip results in a drop in floor elevation of about 7 m between the waste shaft and the southern panel. The computational gridding for BRAGFLO does not include this change in elevation.

The computational grid shown in Fig. 1 extends vertically 645 m from the bottom of the Salado Formation to the top of the Culebra Dolomite Member of the Rustler Formation and extends horizontally for approximately 29 km. Stratigraphic units included in the grid are the intact halite of the Salado Formation, Marker Bed 139, Anhydrite Layers A and B, which are represented as a single anhydrite layer, and the lower unnamed member of the Rustler Formation and the Culebra Dolomite, which are represented as a single layer. The computational grid also includes a disturbed rock zone, which extends vertically around the repository and includes parts of Marker Bed 139 and Anhydrite Layers A and B. The permeability of the disturbed rock zone was assumed to sufficiently low (i.e., 2.41×10^{-20} m^2, which is an order of magnitude above the assumed permeability of 2.41×10^{-21} m^2 for halite in the Salado Formation) to prevent significant gas flow around the panel seals.

The computational cells used with BRAGFLO represent two-dimensional projections of three-dimensional features with different volumes. The width of the

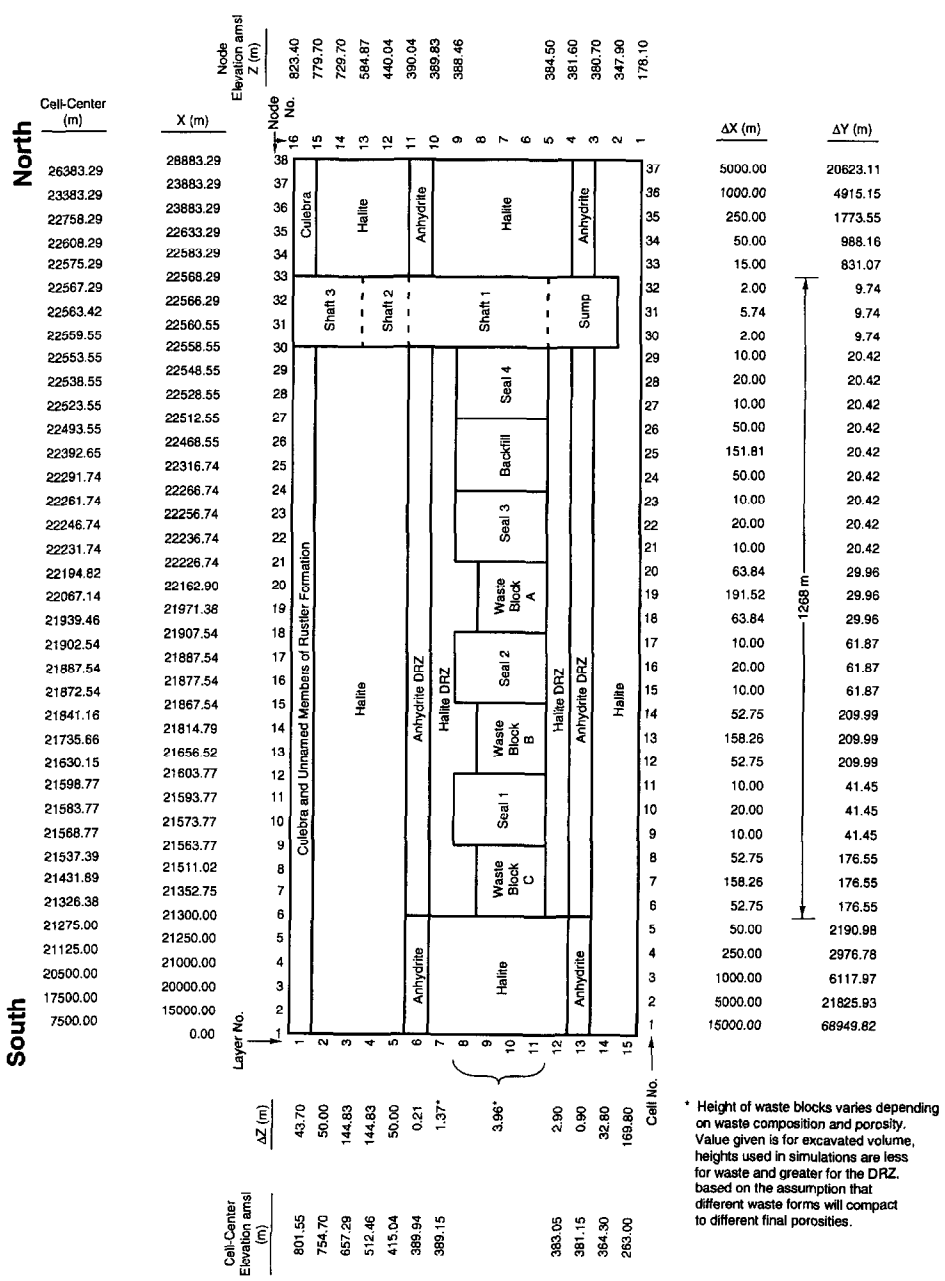

Fig. 1. Gridding scheme employed with BRAGFLO for the two-dimensional vertical cross-section model of the full repository used in analysis of permeable shaft with panel seals.

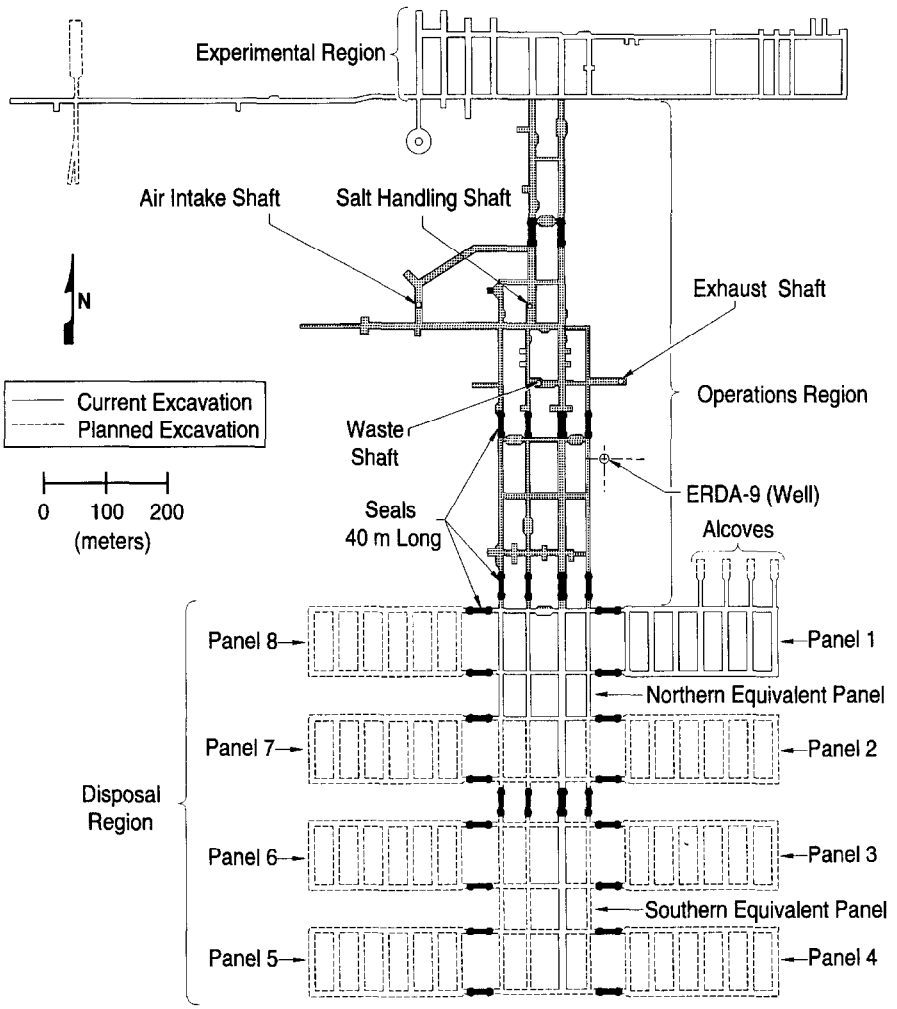

Fig. 2. Excavated areas in the WIPP repository [23, 24].

computational cells (i.e., distance measured in the direction of the y coordinate in Fig. 1, which is perpendicular to the page) varies significantly before projection to two dimensions, from as little as 9.74 m at the location of the shaft to as much as 69 km in the intact Salado Formation. This dimension of the grid does not vary vertically; thus, where the grid is thin near the shaft because of the small excavated volume, all grid elements, including the disturbed rock zone, the intact Salado Formation and the Culebra Dolomite, are given the same value for the y-dimension. Figs. 2–5 and 2–6 of Ref. [17] show enlarged representations of the grid in the horizontal plane containing the repository.

The third dimension (i.e., the y coordinate, which is perpendicular to the page in Fig. 1) is included in the construction of the computational grid to allow for different

storage volumes for brine and gas in each cell. Flow is not modeled in the third dimension and occurs only in the plane of Fig. 1 (i.e., in the directions of the x and z coordinates). Flow from Waste Block C to the Culebra Dolomite, for example, would occur horizontally through the other waste blocks and the panel seals, and then vertically up the shaft.

The ends of the grid, south of Waste Block C and north of the shaft, require additional explanation. The intent was to simulate some three-dimensional behavior with a two-dimension grid. With the repository or shaft acting as sources or sinks, fluid flow will be primarily horizontal, and mostly through the anhydrite layers. Close to the repository, flow paths will have complex orientations because of the variable geometry of the excavations. Further away from the repository, at a distance perhaps several times the maximum horizontal dimension of the repository (about 1.3 km), flow will be nearly radial either toward or away from the sink or source. This cylindrical flow pattern can be approximated with a two-dimensional model if the width of grid blocks (i.e., the y-dimension of Fig. 1) increases away from the source or sink by a factor of $2\pi r$, where r is the distance from the source or sink at the center of the grid [25]. In a strict sense, this relationship is valid only if the entire grid is set up this way, starting from one side. Such a grid represents a vertical cylinder, and the resulting two-dimensional model will simulate radial flow in a three-dimensional cylinder. In the grid used here, only the north and south ends were treated in this fashion, and the results are not exact in modeling all flow outward from the repository/shaft region. However, as a first approximation, this procedure accounts for the radial increase in pore volume away from the central region. This radial increase in pore volume is potentially important because brine and gas flow away from the repository will not be restricted to two dimensions (vertically and in one dimension horizontally). Rather, at a distance of a few kilometers from the repository (approximately the disposal-unit boundary), flow will be radial into an increasing pore volume.

Waste Blocks A, B and C are separated by seal blocks that preserve both the total length and the total volume of the seals located between the panels. Thus, Seals 3 and 4 contain the composite volume of the drift seals north of the waste (Fig. 2). Seal 2 contains the composite volume of the 12 panel seals separating Waste Block A from Waste Block B, and Seal 3 contains the volume of the 8 panel seals separating Waste Block B from Waste Block C. Seals are assumed to have a height equal to that of a newly excavated room, approximately 4 m. Actual heights of seals may vary depending on location. Seals are assumed to occupy only the original volume of the drifts in which they are emplaced, and no correction is made for possible additional excavation, such as downward into Marker Bed 139 during seal construction. All panel and drift seals are assumed to have the same properties.

The single composite shaft is divided into four sections: a sump and three arbitrarily divided higher sections each having different material properties. The three upper sections are used to represent different degrees of consolidation of the halite seals and backfill at different depths, with the deeper sections having lower permeability. The first shaft section above the sump, labeled Shaft 1 in Fig. 1, extends from the bottom of the waste blocks upward to the top of the Anhydrite Layers A and B. The middle shaft

section, labeled Shaft 2 in Fig. 1, extends halfway to the top of the Salado Formation, and the upper section, labeled Shaft 3, extends to the top of the Culebra Dolomite. The lowermost portion of the shaft, the sump, is assumed to be backfilled, and has been included in the model because of its possible role as a brink sink. The modeled sump extends downward 36.6 m from the repository floor, resulting in a modeled volume larger than that of the actual sumps. Two of the four shafts have no sumps, and depths in the other two are 38.4 m (Waste Shaft) and 33.5 m (Salt Handling Shaft) [24]. However, the pore volume of the sump is small relative to the volume in the entire shaft. The disturbed rock zone is modeled only above and below the waste, drift and panel seal, and backfill blocks.

No mass is allowed to cross the far-field outer boundary of the grid except for the northern- and southernmost cells of the Culebra Dolomite. Fixed-pressure boundaries are defined for those locations to approximate the observed head in the Culebra. The initial pressure throughout the Culebra, including the lateral boundary cells, was set at 1.053 MPa. Initial brine saturation in the Culebra was set to 1.0 (i.e., there is no initial gas in the Culebra). Any gas that does eventually appear in the Culebra must come from the waste or from gas initially in the shaft or drift blocks.

Initial far-field pressures in the Salado Formation, including halite and anhydrite layers, were varied hydrostatically relative to a specified value at the level of Marker Bed 139, with the assumption of a brine density of 1230 kg/m^3. Initial pressure in Marker Bed 139 is one of the imprecisely known variables considered in the uncertainty/sensitivity analysis. Initial pressure in the waste, seals and backfill was assumed to be atmospheric (0.101 MPa). Initial pressure was assumed to be constant horizontally throughout any given layer in all of its constituent materials. The Salado Formation halite, the anhydrite, and the disturbed rock zone were assumed to be initially fully brine saturated.

Initial conditions in the shafts and drifts are uncertain, and two sets of calculations were carried out to evaluate the effects of assuming initial full brine saturation and initial full gas saturation. In the first set, the shaft seals, drift seals and backfill were assumed to be gas saturated, and initial pressure was atmospheric, 0.101 MPa. In the second set, these regions were assumed to be brine saturated fully, with the initial pressure in the drift seals and backfill equal to atmospheric. The initial brine pressure in the shaft was hydrostatic, varying with depth relative to the sampled value for the pressure in Marker Bed 139. In both sets of calculations, the initial shaft pressure extends to the top of the Salado Formation, with the result that a difference exists between the shaft and the Culebra pressures. For the gas-saturated shaft, this initial pressure difference was −0.95 MPa, compared to a range from 3.9 to 4.5 MPa for the brine-saturated shaft. This difference in gradient could cause different early-time behavior in the calculations for gas-saturated and brine-saturated shafts. Because the shaft was brine-saturated in either case within about 150 yr, results over 10 000 yr were relatively insensitive to the initial gas saturation of the drifts and shafts. The results contained in this presentation were obtained with the assumption of an initially gas-saturated shaft; results obtained with the assumption of an initially brine-saturated shaft are given in Ref. [17].

3. Mathematical description

A brief mathematical description of the models in use is now presented. This description is adapted from more extensive descriptions in Refs. [16, 21] and is presented here to provide the reader with an accessible description of the mathematical formulation of the problem under study.

The following system of three equations is used to represent two-phase (i.e., brine and gas) flow [16, Section 3.1]:

$$\frac{\partial}{\partial x}\left[H\frac{\rho_n k k_{rn}}{\mu_n}\frac{\partial(P_n-\rho_n g D)}{\partial x}\right]+\frac{\partial}{\partial z}\left[H\frac{\rho_n k k_{rn}}{\mu_n}\frac{\partial(P_n-\rho_n g D)}{\partial z}\right]+Hq_n+Hq_{rn}$$
$$=H\left[\rho_n S_n\phi\beta_s\frac{\partial P_w}{\partial t}+\phi S_n\frac{\partial\rho_n}{\partial t}+\phi\rho_n\frac{\partial S_n}{\partial t}\right], \tag{1}$$

$$\frac{\partial}{\partial x}\left[H\frac{\rho_w k k_{rw}}{\mu_w}\frac{\partial(P_w-\rho_w g D)}{\partial x}\right]+\frac{\partial}{\partial z}\left[H\frac{\rho_w k k_{rw}}{\mu_w}\frac{\partial(P_w-\rho_w g D)}{\partial z}\right]+Hq_w+Hq_{rw}$$
$$=H\left[\rho_w S_w\phi\beta_s\frac{\partial P_w}{\partial t}+\phi S_w\frac{\partial\rho_w}{\partial t}+\phi\rho_w\frac{\partial S_w}{\partial t}\right], \tag{2}$$

$$\beta_s=\frac{1}{\phi}\frac{\partial\phi}{\partial P_w}, \tag{3}$$

where D is the depth (m) measured from surface, g the acceleration due to gravity (m/s^2), H the geometric factor (m), k the permeability (m^2), k_{rl} the relative permeability (dimensionless) to phase l ($l = n$, nonwetting phase, $l = w$, wetting phase), P_l the pressure of phase l (Pa), q_l the rate of injection (or removal, if negative) of phase l ($kg/m^3 s$), q_{rl} the rate of production (or consumption, if negative) of phase l due to chemical reaction ($kg/m^3 s$), S_l the saturation of phase l (dimensionless), t the time (s), x the coordinate in x (i.e., horizontal) direction, z the coordinate in z (i.e., vertical) direction, β_s the matrix compressibility (Pa^{-1}), ϕ the porosity (dimensionless), ρ_l the density of phase l (kg/m^3), and μ_l the viscosity of phase l (kg/ms).

The wetting phase is assumed to consist of only brine and the nonwetting phase is assumed to consist of only gas. The functions P_n and P_w represent the pressures that would be exerted by the nonwetting and wetting phases, respectively, given that they were present; the saturations S_n and S_w are used to specify whether or not these phases are present and hence whether or not these pressures are actually realized. Additional background on the two-phase flow is provided by Crichlow [26] and Peaceman [27] and also in Section 5.2 and Appendix A of Ref. [12].

The preceding reduces to a system of three equations in three unknowns (i.e., P_w, S_n, ϕ) through the assumption of the Brooks–Corey relationship [13, Section 2.3.1],

$$P_n=P_w+\left(\frac{1-S_n-S_{wr}}{1-S_{nr}-S_{wr}}\right)^{-1/\lambda}P_t, \tag{4}$$

and the saturation constraint

$$S_w = 1 - S_n, \tag{5}$$

where P_t is the threshold displacement pressure (Pa), S_{nr} the residual saturation of nonwetting phase (dimensionless), S_{wr} the residual saturation of wetting phase (dimensionless), and λ the Brooks–Corey pore size distribution parameter (dimensionless).

In the present analysis, $S_{nr} = 0.07$, $S_{wr} = 0.276$ and $\lambda = 2.89$ in the waste [13, Section 3.4.4], $S_{nr} = 0.2$, $S_{wr} = 0.2$ and $\lambda = 0.7$ in all other regions, and P_t is a function of permeability. A well-defined relationship exists between permeability k and threshold displacement pressure P_t (Fig. 2.3-1 of Ref. [13] as adapted from Figs. 5 and 8, of Ref. [27]). In particular, the fitting of a regression model yields

$$P_t(k) = 5.6 \times 10^{-7} k^{-0.346}. \tag{6}$$

In the present analysis, the preceding relationship is used to define P_t for all regions except the waste blocks, where the relationship $P_t = 0$ Pa is assumed to hold.

The values used for k, k_{rn}, k_{rw}, ρ_n, ρ_w, μ_n, μ_w and β_s are summarized in Table 1. The variable H appearing in Eqs. (1) and (2) is defined by

$$H = 2\pi x, \tag{7}$$

and provides a correction in the model formulation for the conversion from a three-dimensional geometry [21, Fig. 1] to a two-dimensional geometry as shown in Fig. 1.

Gas production is assumed to result from corrosion of steel and microbial degradation of cellulosics. Thus, the gas generation rate q_{rn} is of the form

$$q_{rn} = q_{rnc} + q_{rnm}, \tag{8}$$

where q_{rnc} is the rate of gas production due to corrosion of steel (kg/m^3 s) and q_{rnm} is the rate of gas production due to microbial degradation of cellulosics (kg/m^3 s).

Gas generation takes place only within the waste panels and all the generated gas is assumed to be H_2. Further, q_{rw} is used to describe the consumption of brine during the corrosion process. The rates q_{rnc}, q_{rnm} and q_{rw} are defined by [13, Sections 3.3.8, 3.3.9]

$$q_{rnc} = (r_{ci} D_s S_w + r_{ch} D_s S_n^*) M(H_2), \tag{9}$$

$$q_{rnm} = (r_{mi} D_c S_w + r_{mh} D_c S_n^*) M(H_2), \tag{10}$$

and

$$q_{rw} = -q_{rnc} X_c(H_2O|H_2) M(H_2O)/M(H_2), \tag{11}$$

where D_s is the surface area density of steel in repository ((m^2-surface area steel)/(m^3-repository)), D_c is the mass density of cellulosics in repository ((kg-cellulosics)/(m^3-repository)), $M(H_2)$ represents kilograms per mole for H_2 (kg/mol) and $M(H_2O)$ represents kilograms per mole for H_2O (kg/mol). Also r_{ch} is the rate of H_2 production by corrosion of steel under humid conditions (mol H_2/(m^2-surface area steel)s), r_{ci} the rate of H_2 production by corrosion of steel under inundated conditions (mol H_2/(m^2-surface area steel)s), r_{mh} the rate of H_2 production by microbial degradation of

Table 1
Values of k, k_m, k_{rw}, β_s, μ_n, μ_w, ρ_n and ρ_w used with BRAGFLO to determine the effects of seal permeabilities and gas generation parameters on gas flow through the repository and up the shaft to the Culebra Dolomite

$k = 2.18 \times 10^{-13}\ m^2$	in Culebra (spatially averaged value derived from transmissivity fields associated with variable CULTRFLD in Ref. [15, Table VIII]
$= 2.41 \times 10^{-21}\ m^2$	in undisturbed halite [13, Section 2.3.5]
$= 2.41 \times 10^{-20}\ m^2$	in disturbed halite ($10 \times$ value for undisturbed halite)
$= k_A$	in undisturbed anhydrite (uncertain input variable; see variable MBPERM in Table 2)
$= 10k_A$	in disturbed anhydrite
$= k_B$	in backfill (uncertain input variable; see variable BFPERMF in Table 2)
$= k_S$	in seals (uncertain input variable; see variable SEALPERM in Table 2)
$= k_{Sh1}$	in lower shaft section (Shaft 1) (uncertain input variable; see variable SH1PERM in Table 2)
$= k_{Sh2}$	in middle shaft section (Shaft 2) (uncertain input variable; see variable SH2PERM in Table 2)
$= k_{Sh3}$	in upper shaft section (Shaft 3) (uncertain input variable; see variable SH3PERM in Table 2)
$= 1.1 \times 10^{-13}\ m^2$	in repository [13, Section 3.4.7]

$$k_{rn} = \left[1 - \frac{1 - S_n - S_{wr}}{1 - S_{nr} - S_{wr}}\right]^2 \left[1 - \left(\frac{1 - S_n - S_{wr}}{1 - S_{nr} - S_{wr}}\right)^{(2+\lambda)/\lambda}\right] \quad \text{[13, Eq. 2.3–5]}$$

$$k_{rw} = \left(\frac{1 - S_n - S_{wr}}{1 - S_{nr} - S_{wr}}\right)^{(2+3\lambda)/\lambda} \quad \text{[13, Eq. 2.3–4]}$$

$\beta_s = 1.586 \times 10^{-9}\ Pa^{-1}$	in disturbed halite [17, Table 3.2-1]
$= 7.974 \times 10^{-9}\ Pa^{-1}$	in undisturbed anhydrite [17, Table 3.2-1]
$= 1.191 \times 10^{-9}\ Pa^{-1}$	in disturbed anhydrite [17, Table 3.2-1]
$= 8.423 \times 10^{-10}\ Pa^{-1}$	in waste [17, Table 3.2-1]
$= 1.126 \times 10^{-8}\ Pa^{-1}$	elsewhere [17, Table 3.2-1]

$\mu_n = 9.6 \times 10^{-6}$ Pa s (Ref. [13, p. 4–21] lists a median value of 9.20×10^{-6} Pa s at 300.15 K, 15 MPa)
$\mu_w = 1.8 \times 10^{-3}$ Pa s [13, p. 4–7]
ρ_n: obtained from P_n and solution of Redlich–Kwong–Soave equation of state [13, Eq. 4.1–6]
$\rho_w = 1.23 \times 10^3 \exp\left[2.5 \times 10^{-10}\ (P_w - 1.01325 \times 10^5)\right]$ [13, Eq. 4.1–5]

cellulosics under humid conditions (mol H_2/(kg-cellulosics)s), r_{mi} the rate of H_2 production by microbial degradation of cellulosics under inundated conditions (mol H_2/(kg-cellulosics)s),

$$S_n^* = \begin{cases} S_n & \text{if } S_w > 0, \\ 0 & \text{if } S_w = 0, \end{cases} \tag{12}$$

and $X_c(H_2O|H_2)$ the stoichiometric term for consumption of H_2O by corrosion of steel (mol H_2O/mol H_2).

The products $r_{ci}D_s$, $r_{ch}D_s$, $r_{mi}D_c$ and $r_{mh}D_c$ in Eqs. (9) and (10) define constant rates of gas generation (units: mol/m^3 s) that continue until the associated substrate (i.e., steel or cellulosics) is exhausted. The terms S_w and S_n^* in Eqs. (9) and (10), which are functions of location and time, correct for the amount of substrate that is exposed to

inundated and humid conditions, respectively. All corrosion and microbial action is assumed to stop when no brine is present, which is the reason that 0 replaces $S_n = 1$ in the definition of S_n^* in Eq. (12). In the present analysis, r_{ch}, r_{ci}, r_{mh} and r_{mi} are defined by uncertain input variables (see variables GRCORH, GRCORI, GRMICH, GRMICI in Table 2). Further, $M(H_2) = 2.02 \times 10^{-3}$ kg/mol and $M(H_2O) = 1.80 \times 10^{-2}$ kg/mol. The development of D_s, D_c and X_c $(H_2O|H_2)$ is discussed in Ref. [21] and also in Ref. [16], which can be consulted to obtain a complete description of the gas generation model in use.

Eqs. (1)–(3) are solved by BRAGFLO with the Newton–Raphson iteration technique in conjunction with a fully implicit, finite-difference procedure on the computational grid in Fig. 1. The initial value and boundary value conditions used in conjunction with this solution are summarized in Table 3.

The 16 imprecisely known variables listed in Table 2 were used as input to BRAGFLO for the uncertainty and sensitivity studies contained in this presentation. The distributions indicated in Table 2 for the individual variables are characterizing subjective uncertainty [31, 32]. Thus, these distributions characterize a degree of belief as to where the value of a fixed but unknown quantity is located. The analysis used a Latin hypercube sample [33] of size 22 from the 16 variables in Table 2. This sample was generated with the LHS program [34]. Further, the Iman/Conover restricted pairing technique [35] was used to assure that the correlations between the sampled variables were close to zero. The resultant sample is listed in Table 3.2-2b of Ref. [17]. One BRAGFLO calculation was performed for each sample element. Thus, 22 BRAGFLO calculations are available for analysis. The uncertainty and sensitivity analysis results in this presentation are based on an exploration of the relationships between the 22 sample elements and the associated 22 BRAGFLO calculations [19, 20].

A widely used guide for selecting the sample size to use in an uncertainty/sensitivity study based on Latin hypercube sampling is that the number of elements in the sample should equal $4\,nV/3$, where nV is the number of variables in the sample. This rule was used for the present analysis and resulted in the choice of 22 as the sample size. However, the actual basis for this rule is the size of the sample needed for the successful numerical implementation of the Iman/Conover restricted-pairing technique [35] that is used to control the correlation structure within the sample. To the best of the authors' knowledge, a rule for the optimum size of a Latin hypercube sample for use in an uncertainty and sensitivity analysis is not known.

The variables BFPERMF, BRSATF, GRCORHF, GRMICHF, SH2PERMF and SH3PERMF in Table 2 are scale factors that are used in constructing the variable values that are actually used in the analysis. Associated with each of these scale factors in Table 2 is the definition of the variable that is actually used by BRAGFLO. The sensitivity analyses presented in Sections 4–6 use the actual BRAGFLO inputs (i.e., BFPERM, BRSAT, GRCORH, GRMICH, SH2PERM and SH3PERM) rather than the corresponding scale factors. The transformed variables (i.e., actual BRAGFLO inputs) are used because of the relatively complex relationships involving BFPERMF, SH2PERMF and SH3PERMF.

Gas flow through the repository and up the shaft to the Culebra Dolomite is the outcome of greatest interest in this analysis. Thus, a natural starting point is an

Table 2
Imprecisely known variables used in BRAGFLO to determine the effects of seal permeabilities and gas generation parameters on gas flow through the repository and up the shaft to the Culebra Dolomite

Variable	Definition
BFPERMF	Scale factor used in the definition of permeability of backfill in waste panels (dimensionless). Range, 0–1; median, 0.5, distribution, normal. Actual backfill permeability, BFPERM, is defined by $\log \text{BFPERM} = \log \text{SEALPERM} + (-14 - \log \text{SEALPERM})\ \text{BFPERMF}.$ BFPERM defines variable k in Eqs. (1) and (2) for region labeled "Backfill" in Fig. 1 (i.e., BFPERM is the variable k_B in Table 1). Additional information: Ref. [17, Section 3.2.2] Variable 13 in Latin hypercube sample (LHS)
BRSATF	Scale factor used in definition of initial brine saturation of waste (dimensionless). Range, 0–1; median, 0.5, distribution, uniform. Actual value for initial brine saturation of waste, BRSAT, is $\text{BRSAT} = 0.276\text{BRSATF}.$ BRSAT defines variable S_{pan} in Eq. (23) of Ref. [21]. Additional information: Ref. [13, Section 3.4.9]. Variable 1 in LHS
GRCORHF	Scale factor used in definition of gas generation rate for corrosion of steel under humid conditions (dimensionless). Range, 0 to 5×10^{-1}; median, 1×10^{-1}, distribution, piecewise uniform. Actual generation rate, GRCORH, is $\text{GRCORH} = \text{GRCORHF} \cdot \text{GRCORI}.$ GRCORH defines variable r_{ch} in Eq. (9). Additional information: Memo from Brush, 8 July 1991, contained in Ref. [13, Appendix A] and Ref. [13, Section 3.3.8]. Variable 3 in LHS
GRCORI	Gas-generation rate for corrosion of steel under inundated conditions (mol/m^2 surface area steel s). Defines variable r_{ci} in Eq. (9). Range, 0 to 1.3×10^{-8} mol/m^2 s; median, 6.3×10^{-9} mol/m^2 s; distribution, piecewise uniform. Additional information: same as GRCORHF. Variable 4 in LHS
GRMICHF	Scale factor used in definition of gas-generation rate due to microbial degradation of cellulosics under humid conditions (dimensionless). Range, 0 to 2×10^{-1}; median, 1×10^{-1}; distribution, piecewise uniform. Actual gas-generation rate, GRMICH, is $\text{GRMICH} = \text{GRMICHF} \cdot \text{GRMICI}.$ GRMICH defines variable r_{mh} in Eq. (10). Additional information: same as GRCORHF. Variable 5 in LHS
GRMICI	Gas-generation rate due to microbial degradation of cellulosics under inundated conditions (mol/kg cellulosics s). Defines variable r_{mi} in Eq. (10). Range, 0 to 1.6×10^{-8} mol/kg s; median, 3.2×10^{-9} mol/kg s; distribution, piecewise uniform. Additional information: same as GRCORHF. Variable 6 in LHS
MBPERM	Permeability in anhydrite marker beds in Salado Formation under undisturbed conditions (m^2). Defines variable k in Eqs. (1) and (2) for regions labeled "Anhydrite" in Fig. 1 (i.e., MBPERM is the variable k_A in Table 1). Range, 8.5×10^{-21} to 1.8×10^{-18} m^2; median, 7.8×10^{-20} m^2; distribution, piecewise uniform. Additional information: memo from Beauheim, 14 June 1991, contained in Ref. [13, Appendix A] and Ref. [13, Section 2.4.5]. Variable 11 in LHS
MBPRES	Pressure in anhydrite marker beds in Salado Formation under undisturbed conditions (Pa). Defines variable $P_w(0)$ in Table 3. Range, 8.21×10^6 to 1.48×10^7 Pa; median, 1.28×10^7 Pa; distribution, piecewise uniform. Additional information: memos from Beauheim, 14 June 1991, and Howarth, 12 June 1991, contained in Ref. [13, Appendix A] and Ref. [13, Section 2.4.6]. Variable 10 in LHS

Table 2. Continued

Variable	Definition
SEALPERM	Permeability of seals between waste blocks in repository (m^2). Defines variable k in Eqs. (1) and (2) for regions labeled "Seal 1", "Seal 2", "Seal 3" and "Seal 4" in Fig. 1 (i.e., SEALPERM is the variable k_S in Table 1). Range, 3.3×10^{-21} to 1×10^{-14} m^2; median, 5.7×10^{-18} m^2; distribution, lognormal. Additional information: Ref. [17, Section 3.2.2] and Ref. [13, Section 3.2.2]. Variable 12 in LHS
SH1PERM	Permeability of lower shaft section (m^2). Defines variable k in Eqs. (1) and (2) for region labeled "Shaft 1" in Fig. 1 (i.e., SH1PERM is the variable k_{Sh1} in Table 1). Range, 3.3×10^{-21} to 1×10^{-14} m^2; median, 5.7×10^{-18} m^2; distribution, lognormal. Additional information: Ref. [17, Section 3.2.2]. Variable 14 in LHS
SH2PERMF	Scale factor used in definition of permeability of middle shaft section. Range, 0–1; median, 0.5; distribution, normal. Actual permeability of middle shaft section, SH2PERM, is defined by $\log \text{SH2PERM} = \log \text{SH1PERM} + (-14 - \log \text{SH1PERM})\ \text{SH2PERMF}.$ SH2PERM defines variable k in Eqs. (1) and (2) for region labeled "Shaft 2" in Fig. 1 (i.e., SH2PERM is the variable k_{Sh2} in Table 1). Additional information: Ref. [17, Section 3.2.2]. Variable 15 in LHS
SH3PERMF	Scale factor used in definition of permeability of upper shaft section. Range, 0–1; median; 0.5; distribution, normal. Actual permeability of upper shaft section, SH3PERM, is defined by $\log \text{SH3PERM} = \log \text{SH2PERM} + (-14 - \log \text{SH2PERM})\ \text{SH3PERMF}.$ SH3PERM defines variable k in Eqs. (1) and (2) for region labeled "Shaft 3" in Fig.1 (i.e., SH3PERM is the variable k_{Sh3} in Table 1). Additional information: Ref. [17, Section 3.2.2]. Variable 16 in LHS
STOICCOR	Stoichiometric factor for corrosion of steel (dimensionless). The most plausible corrosion reactions after closure of the WIPP are believed to be $Fe + 2H_2O = Fe(OH)_2 + H_2$ and $3Fe + 4H_2O = Fe_3O_4 + 4H_2$, although there exists substantial uncertainty as to what the proportions of these two reactions might be [29; 13, Section 3.3.8]. The average stoichiometry of the preceding reactions is $Fe + [(4 + 2X)/3]H_2O = [(4 - X)/3]H_2 + [X]Fe(OH)_2 + [(1 - X)/3]Fe_3O_4,$ where X and $1 - X$ are the fractions of iron consumed in the two reactions. The stoichiometric term $X_c(H_2O\|H_2)$ in Eq. (11) for the consumption of H_2O by the corrosion of steel is given by $X_c(H_2O\|H_2) = (4 + 2X)/(4 - X).$ STOICCOR defines X in the preceding equation and thus $X_c(H_2O\|H_2)$ in Eq. (11). Range, 0–1; median, 5×10^{-1}; distribution, uniform. Additional information: Brush and Anderson in Ref. [7, p. A-6] and Ref. [13, Section 3.3.8]. Variable 2 in LHS
STOICMIC	Stoichiometric coefficient for microbial degradation of cellulosics (i.e., moles of gas, which is assumed to be H_2, produced per mole of cellulose, CH_2O, undergoing microbial degradation). Defines variable $M(H_2\|CH_2O)$ in Eq. (71) of Ref. [16], which can be consulted for more detail on the implementation of the gas-generation model used in this analysis. Range, 0–1.67 mol/mol; median, 8.35×10^{-1} mol/mol; distribution, uniform. Additional information: Brush and Anderson in Ref. [7, p. A-10] and Ref. [13, Section 3.3.9]. Variable 9 in LHS

Table 2. Continued

Variable	Definition
VMETAL	Fraction of total waste volume that is occupied by IDB (integrated data base) [30] metals and glass waste category (dimensionless). Defines variable f_m in Eq. (58) of Ref. [16] and is used in determination of amount of steel undergoing corrosion. Range, 2.76×10^{-1} to 4.76×10^{-1}; median, 3.76×10^{-1}; distribution, normal. Additional information: Ref. [13, Section 3.4.1]. Variable 7 in LHS
VWOOD	Fraction of total waste volume that is occupied by IDB combustible waste category (dimensionless). Defines variable f_c in Eq. (15) of Ref. [21] and is used in determination of amount of cellulose undergoing microbial degradation. Range, 2.84×10^{-1} to 4.84×10^{-1}; median, 3.84×10^{-1}; distribution, normal. Additional Information: Ref. [13, Section 3.4.1]. Variable 8 in LHS

Table 3
Initial value and boundary value conditions used with BRAGFLO and computational grid in Fig. 1

Initial value conditions
$P_w(x, z, 0) = 1.053 \times 10^6$ Pa in Culebra
$= 1.032 \times 10^5$ Pa (i.e., atmospheric pressure) in waste blocks, seals, backfill and shaft
$= P_w(0) + \rho_B g[z_{MB} - z]$ elsewhere, where ρ_B = density of brine (1230 kg/m^3), z_{MB} = center of Marker Bed 139 (381.15 m), g = acceleration due to gravity (9.81 m/s^2), (x, z) is a point for which the initial value of $P_w(x, z, 0)$ has not already been defined, and $P_w(0)$ is an uncertain input variable (see variable MBPRES in Table 2)
$S_n(x, z, 0) = 1 - S_w(0)$ in waste blocks, where $S_w(0)$ is a function of the uncertain input variable BRSAT in Table 2 (see Ref. [21, Eq. (23)])
$= 1$ in shaft seals, sump, drift seals and backfill
$= 0$ otherwise
$\phi(x, z, 0) = 0.139$ in Culebra (median value, Ref. [13, Section 2.6.4])
$= 0.01$ in undisturbed halite and anhydrite (median value, Ref. [13, Section 2.3.7])
$= 0.055$ in disturbed anhydrite (median value, Ref. [13, Section 2.4.7])
$= 0.06$ in disturbed halite (median value, Ref. [13, Section 2.3.7])
$= \phi_r(0)$ in repository (see Ref. [21, Eq. (22)])
$= 0.01$ in backfill, panel seals, shaft seals and sump
Boundary value conditions
Boundaries above ($z = 823.4$ m) and below ($z = 178.1$ m) system
$\partial S_n(x, 823.4, t)/\partial z = \partial P_w(x, 823.4, t)/\partial z = 0$ for $0 \leqslant x \leqslant 28883.29$ m, $0 \leqslant t$
$\partial S_n(x, 178.1, t)/\partial z = \partial P_w(x, 178.1, t)/\partial z = 0$ for $0 \leqslant x \leqslant 28883.29$ m, $0 \leqslant t$
Boundary on left ($x = 0$ m) of system
$\partial S_n(0, z, t)/\partial x = \partial P_w(0, z, t)/\partial x = 0$ for $178.1 \leqslant z \leqslant 779.7$ m, $0 \leqslant t$
$P_n(0, z, t)^a = P_w(0, z, t) = 1.053 \times 10^6$ Pa for $779.7 < x \leqslant 823.4$ m
Boundary on right ($x = 28883.29$ m) of system
$\partial S_n(28883.29, z, t)/\partial x = \partial P_w(28883.29, z, t)/\partial x = 0$ for $178.1 \leqslant z \leqslant 779.7$ m, $0 \leqslant t$
$P_n(28883.29, z, t)^a = P_w(28883.29, z, t) = 1.053 \times 10^6$ Pa for $779.7 < z \leqslant 823.4$ m, $0 \leqslant t$

[a] With $S_n(0, z, t)$ and $S_n(28883.29, z, t)$ defined by Eqs. (4)–(5).

exploration of gas generation. Uncertainty and sensitivity analysis results related to corrosion, microbial degradation and total gas production are presented in Section 4. Then, gas saturation and gas pressure in the individual waste blocks are investigated in Section 5. Finally, gas migration through the shaft to the Culebra Dolomite is considered in Section 6.

4. Gas generation

A summary of the results for gas generation due to corrosion is given in Fig. 3. The three left frames in Fig. 3 show cumulative gas generation for the entire repository as a function of time due to corrosion under humid conditions (upper left frame), corrosion under inundated conditions (middle left frame) and corrosion under either humid or inundated conditions (lower left frame). Each curve in these frames results from a single Latin hypercube sample element (i.e., each frame has 22 curves, one for each sample element). The range of gas production values under humid and inundated conditions tends to be similar, which implies that neither of the two corrosion conditions is dominating gas generation. The lower left frame is showing the total gas production due to corrosion that takes place in the repository.

Formal sensitivity analysis techniques based on partial rank correlation [19, 20] can be used to investigate the variation in cumulative gas production shown in Fig. 3. As indicated by the (rank) correlation matrix

SEALPERM	1.00				
BFPERM	0.54	1.00			
SH1PERM	0.00	0.04	1.00		
SH2PERM	− 0.03	− 0.01	0.64	1.00	
SH3PERM	0.05	0.11	0.52	0.80	1.00
	SEALPERM	BFPERM	SH1PERM	SH2PERM	SH3PERM

(13)

the transformations given in Table 2 result in substantial correlations between SEALPERM and BFPERM and also between SH1PERM, SH2PERM and SH3PERM. In initial analyses based on partial rank correlation coefficients (PRCCs), these correlations tended to produce unstable and ambiguous results. In particular, with 16 sampled variables, a sample size of 22 and correlations between variables, there is often little information left to characterize with a partial correlation coefficient after the correction is made for the effects of the other variables (e.g., see [36, Sections IX.1, IX.2] and [37]). To reduce the problems resulting from correlated input, the variables BFPERM, SH1PERM and SH3PERM were dropped from the analysis. Rank correlations also exist between GRCORH and GRCORI (i.e., 0.64) and between GRMICH and GRMICI (i.e., 0.68). However, these correlations did not seem to cause the misleading results that derived from the correlations between SEALPERM and

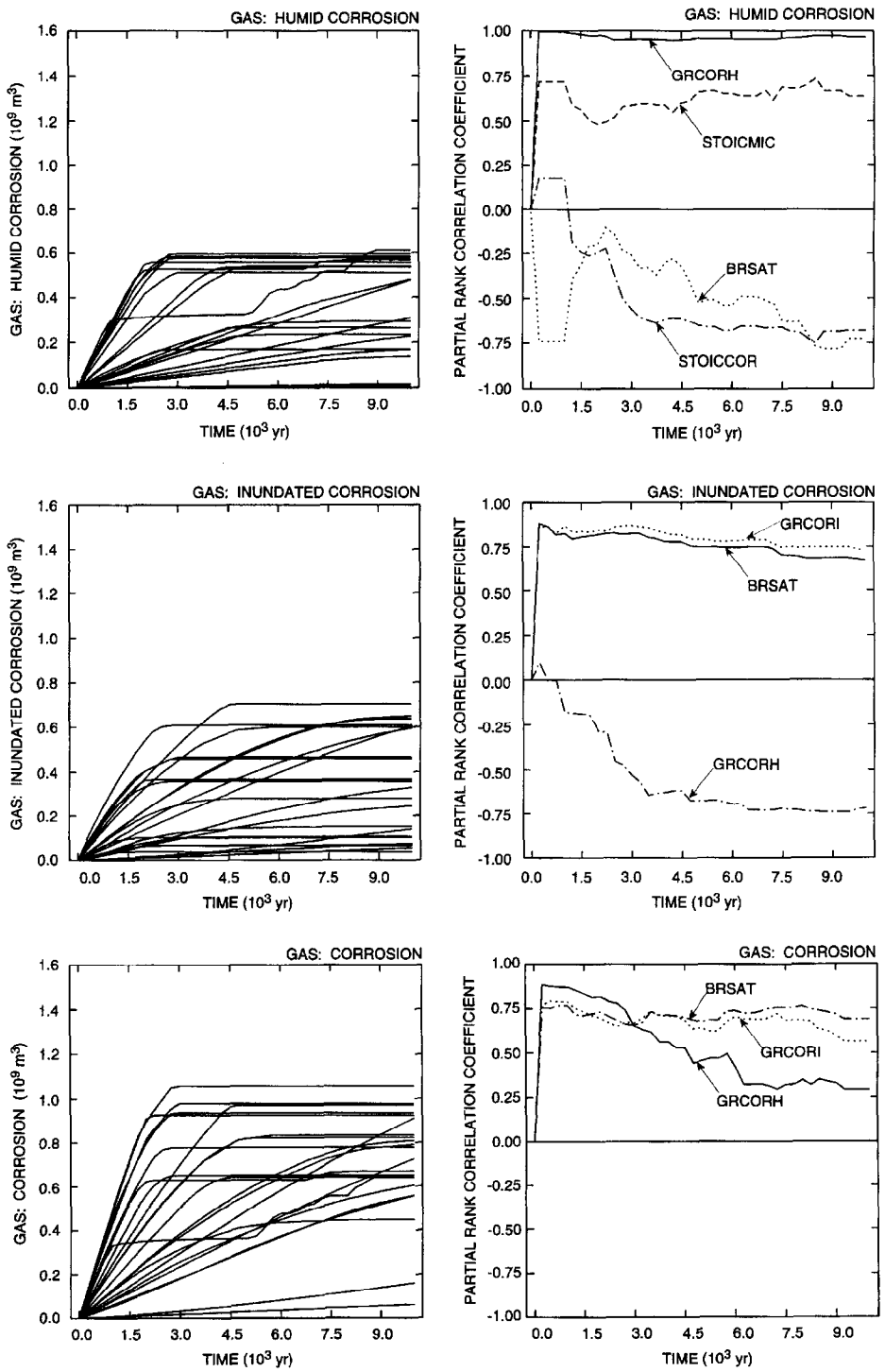

Fig. 3. Uncertainty and sensitivity analysis results for gas generation due to corrosion of steel.

BFPERM and also between SH1PERM, SH2PERM and SH3PERM; thus, the transformed variables GRCORH and GRMICH were left in the partial correlation analysis. As a result, the following 13 variables were used in the calculation of the PRCCs presented as part of this analysis: BRSAT, GRCORH, GRCORI, GRMICH, GRMICI, MBPERM, MBPRES, SEALPERM, SH2PERM, STOICCOR, STOICMIC, VMETAL and VWOOD. The PRCCs contained in this presentation were calculated with the PCCSRC program [38].

The three right frames in Fig. 3 show time-dependent plots of PRCCs between cumulative gas production and individual variables. The PRCCs in Fig. 3 and other similar figures in this presentation are calculated on the basis of vertical slices through the corresponding curves to the left of the PRCCs. Due to the relatively small sample size in use (i.e., 22 observations for 13 independent variables), an absolute value cutoff of 0.7 is used for the selection of the PRCCS for presentation. Specifically, a variable was included in the plotted results only if its PRCC exceeded 0.7 in absolute value at least one time on the abscissa. As a reminder, a positive PRCC indicates that two variables tend to increase and decrease together, and a negative PRCC indicates that, as one variable increases, the other tends to decrease.

Cumulative gas production due to corrosion under humid conditions is dominated by GRCORH (gas-generation rate for corrosion of steel under humid conditions), with cumulative gas production showing a strong tendency to increase as GRCORH increases. In addition, cumulative gas production due to corrosion under humid conditions tends to increase as STOICMIC (stoichiometric coefficient for microbial degradation of cellulosics) increases and tends to decrease as BRSAT (initial brine saturation of waste) and STOICCOR (stoichiometric factor for corrosion of steel) increase. The positive effect for STOICMIC results from increased gas generation due to microbial degradation of cellulosics, with a resultant increase in the amount of repository pore space that is filled with gas (i.e., humid conditions) rather than with brine (i.e., inundated conditions). The negative effect for STOICCOR results because increasing STOICCOR increases the proportion of low-gas-producing reactions in the corrosion process. The negative effect for BRSAT results because there is a fixed amount of steel in the repository for each sample element. Increasing BRSAT increases the amount of this steel that will be consumed by corrosion under inundated conditions, with the result that the amount of gas that can be produced by corrosion under humid conditions is reduced. The PRCCs for GRCORH are very close to 1, with the result that STOICMIC, STOICCOR and BRSAT are actually making relatively small contributions to the uncertainty in gas generation due to corrosion under humid conditions.

Cumulative gas production due to corrosion under inundated conditions tends to increase as GRCORI (gas-generation rate for corrosion of steel under inundated conditions) and BRSAT increase and tends to decrease as GRCORH increases. The positive effects for GRCORI and BRSAT result because increasing GRCORI increases the rate at which gas is produced by corrosion under inundated conditions and increasing BRSAT increases the amount of steel that will be consumed by corrosion under inundated conditions. The negative effect for GRCORH results because the increased consumption of steel and brine by corrosion under humid

conditions reduces the amount of gas that can be produced by the corrosion of steel under inundated conditions.

For total gas production due to corrosion, increasing each of GRCORI, GRCORH and BRSAT tends to increase gas production. Increasing GRCORI, GRCORH and BRSAT tends to increase the rate of gas production and hence cumulative gas production, with this effect becoming less important at later times due to exhaustion of either steel or brine in the waste panels. Typically, low gas production under humid conditions is associated with higher gas production under inundated conditions and vice versa. As a result, the total gas-production curves tend to lie farther above the abscissa than many of the individual curves for corrosion under humid or under inundated conditions.

Stepwise regression analysis [19, 20] can also be used to analyze the cumulative gas production results shown in Fig. 3. Analyses were initially tried with both raw (i.e., untransformed) and rank-transformed [39] data. As the analyses with rank-transformed data consistently performed as well as or better than the analyses with raw data, the regression analyses contained in this presentation use rank-transformed data. The regression analyses were performed with the STEP program [40]. Variables were required to have an α-value [41] of 0.02 to enter a regression analysis and to have an α-value of 0.05 to be retained in the regression analysis. A considerable amount of discretion was used in the selection of the stopping points for the individual regression analyses and took into account the behavior of R^2-values, α-values, the PRESS criterion [42], and the entry of apparently spurious variables into the analysis.

The three regression analyses at the top of Table 4 are for cumulative gas production over 10 000 yr due to corrosion under humid conditions, under inundated conditions and under humid or inundated conditions, respectively. Thus, these three regression analyses are for the gas production values appearing above 10 000 yr in the three left frames of Fig. 3. The regression analysis for gas production under humid conditions indicates a positive effect (i.e., a positive regression coefficient) for GRCORH, with this variable accounting for 81% of the uncertainty in gas production (i.e., $R^2 = 0.81$). The regression analysis for gas production under inundated conditions did not identify any variables that satisfy the minimum condition to enter the regression model (i.e., an α-value of at least 0.02). Scatter plots of cumulative gas production over 10 000 yr due to corrosion under inundated conditions versus the individual variables in Table 4 show no obvious relationships. The regression analysis for total gas production due to corrosion selected the variables GRCORI and BRSAT, with GRCORI and BRSAT each having a positive effect on gas production. However, the resolution in the regression model is low, with GRCORI and BRSAT accounting for only 55% of the uncertainty in gas production due to corrosion. Examination of scatter plots showed that no individual variable exerted a strong influence on cumulative gas production over 10 000 yr due to corrosion (e.g., see Figs. 3–5 of Ref. [18]). However, the actual uncertainty in total gas production due to corrosion is rather small in this analysis, with most values falling between 0.4×10^9 and 1.0×10^9 mol.

A summary of the analysis results for gas generation in the entire repository due to microbial degradation of cellulosics is given in Fig. 4. The three left frames in Fig. 4

Table 4
Stepwise regression analysis with rank-transformed data for cumulative gas production over 10000 yr

Humid corrosion				Inundated corrosion			Total corrosion		
Step[a]	Variable[b]	SRC[c]	R^{2d}	Variable[b]	SRC[c]	R^{2d}	Variable[b]	SRC[c]	R^{2d}
1	GRCORH	0.90	0.81	No variables selected			GRCORI	0.56	0.32
2							BRSAT	0.48	0.55
Humid Microbial				**Inundated Microbial**			**Total Microbial**		
Step[a]	Variable[b]	SRC[c]	R^{2d}	Variable[b]	SRC[c]	R^{2d}	Variable[b]	SRC[c]	R^{2d}
1	STOICMIC	0.69	0.57	STOICMIC	0.79	0.68	STOICMIC	0.95	0.91
2	GRMICH	0.34	0.68	BRSAT	0.33	0.79			
3				GRCORH	−0.24	0.85			
Corrosion and Microbial									
Step[a]	Variable[b]	SRC[c]	R^{2d}						
1	STOICMIC	0.57	0.33						

[a] Steps in stepwise regression analysis.
[b] Variables listed in order of selection in regression analysis.
[c] Standardized regression coefficients (SRCs) in final regression model.
[d] Cumulative R^2 value with entry of each variable into regression model.

show cumulative gas generation due to microbial degradation under humid conditions (upper left), under inundated conditions (middle left) and under humid or inundated conditions (lower left), respectively. As comparison with Fig. 3 shows, gas generation due to microbial degradation is approximately 50% or less of the gas generation due to corrosion. Gas production due to microbial degradation has more curves close to zero than gas production due to corrosion due to the assignment of a range of possible values for STOICMIC that extends to zero, which results in no gas generation due to microbial degradation. The range of cumulative gas generation shown in Fig. 4 for microbial degradation of cellulosics is slightly larger for inundated than for humid conditions.

The right frames in Fig. 4 present sensitivity analysis results based on PRCCs as in Fig. 3. For cumulative gas production under humid conditions, increasing each of STOICMIC, GRMICH (gas-generation rate due to microbial degradation of cellulosics under humid conditions) and VWOOD (fraction of total waste volume occupied by IDB combustible waste category) increases gas production and increasing BRSAT decreases gas production. The positive effects for STOICMIC, GRMICH and VWOOD result because increasing STOICMIC increases the amount of gas produced per unit of cellulose consumed, increasing GRMICH increases the rate of microbial degradation under humid conditions, and increasing VWOOD increases the amount

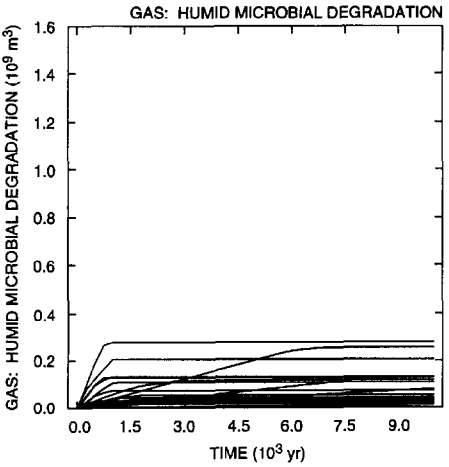
GAS: HUMID MICROBIAL DEGRADATION
GAS: HUMID MICROBIAL DEGRADATION (10^9 m^3)
1.6
1.4
1.2
1.0
0.8
0.6
0.4
0.2
0.0
0.0 1.5 3.0 4.5 6.0 7.5 9.0
TIME (10^3 yr)

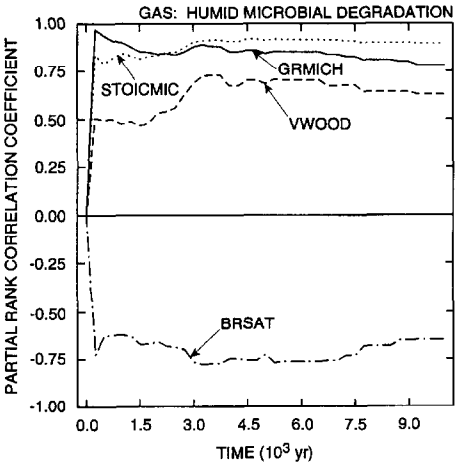
GAS: HUMID MICROBIAL DEGRADATION
PARTIAL RANK CORRELATION COEFFICIENT
1.00
0.75
0.50
0.25
0.00
-0.25
-0.50
-0.75
-1.00
STOICMIC
GRMICH
VWOOD
BRSAT
0.0 1.5 3.0 4.5 6.0 7.5 9.0
TIME (10^3 yr)

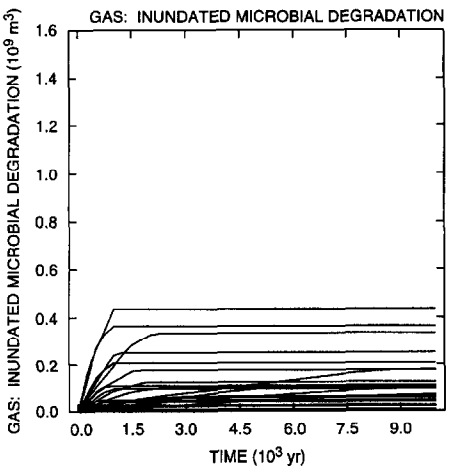
GAS: INUNDATED MICROBIAL DEGRADATION
GAS: INUNDATED MICROBIAL DEGRADATION (10^9 m^3)
1.6
1.4
1.2
1.0
0.8
0.6
0.4
0.2
0.0
0.0 1.5 3.0 4.5 6.0 7.5 9.0
TIME (10^3 yr)

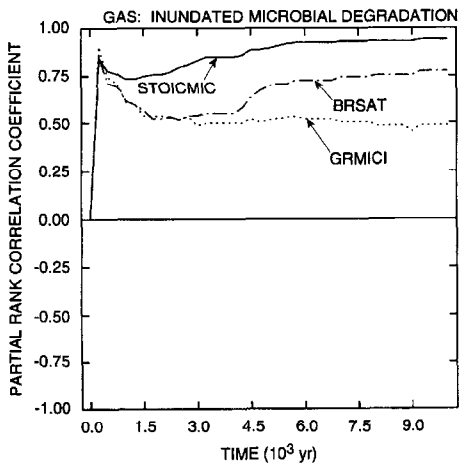
GAS: INUNDATED MICROBIAL DEGRADATION
PARTIAL RANK CORRELATION COEFFICIENT
1.00
0.75
0.50
0.25
0.00
-0.25
-0.50
-0.75
-1.00
STOICMIC
BRSAT
GRMICI
0.0 1.5 3.0 4.5 6.0 7.5 9.0
TIME (10^3 yr)

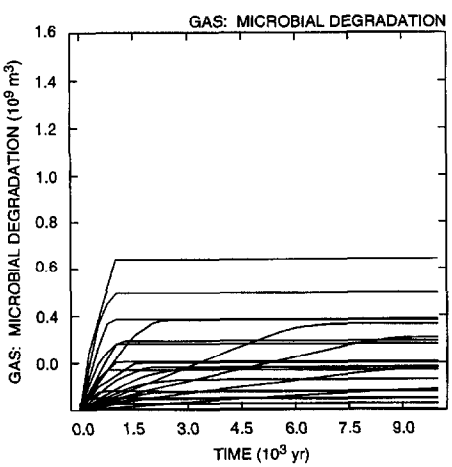
GAS: MICROBIAL DEGRADATION
GAS: MICROBIAL DEGRADATION (10^9 m^3)
1.6
1.4
1.2
1.0
0.8
0.6
0.4
0.0
0.0 1.5 3.0 4.5 6.0 7.5 9.0
TIME (10^3 yr)

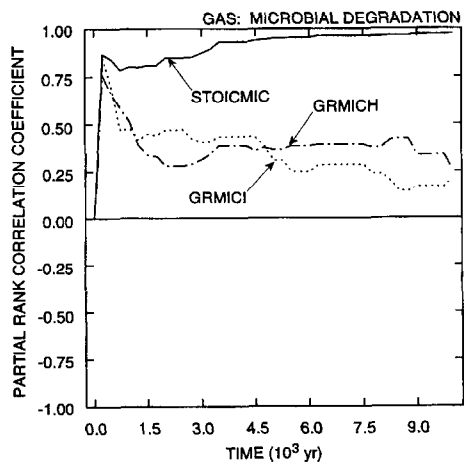
GAS: MICROBIAL DEGRADATION
PARTIAL RANK CORRELATION COEFFICIENT
1.00
0.75
0.50
0.25
0.00
-0.25
-0.50
-0.75
-1.00
STOICMIC
GRMICH
GRMICI
0.0 1.5 3.0 4.5 6.0 7.5 9.0
TIME (10^3 yr)

of cellulose available for microbial degradation. In contrast, increasing BRSAT decreases the amount of gas produced under humid conditions by increasing the amount of cellulosics that will be consumed under inundated conditions. For cumulative gas production under inundated conditions, increasing each of STOICMIC, BRSAT and GRMICI (gas-generation rate due to microbial degradation of cellulosics under inundated conditions) increases gas production. Increasing STOICMIC increases the amount of gas produced per unit of cellulose consumed; increasing BRSAT increases the amount of cellulose that will be consumed under inundated conditions, and increasing GRMICI increases the rate of microbial degradation under inundated conditions. The dominant variable for cumulative gas production due to microbial degradation is STOICMIC, which has an increasingly important positive effect with time and ultimately dominates the variability in cumulative gas production. The variables GRMICI and GRMICH also have positive effects at early times and then decrease in importance.

The three regression analyses in the center of Table 4 are for cumulative gas production over 10 000 yr due to microbial degradation under humid conditions, under inundated conditions and under humid or inundated conditions, respectively. Thus, these regression analyses are for the gas-production values appearing above 10 000 yr in the left frames of Fig. 4. For gas production under humid conditions, the variables STOICMIC and GRMICH can account for 68% of the observed uncertainty in gas production, with gas production tending to increase with increasing values for STOICMIC and GRMICH. For gas production under inundated conditions, the variables STOICMIC and BRSAT can account for 79% of the observed uncertainty in gas production, with gas production tending to increase as each of these variables increases. When the additional variable GRCORH is added to the regression model, 85% of the uncertainty in gas production can be accounted for, with gas production tending to decrease as GRCORH increases because increased gas production tends to decrease the fraction of the pore volume that is filled with brine and hence reduce the amount of microbial degradation that takes place under inundated conditions. For total gas production, the regression analysis identified only the variable STOICMIC. However, STOICMIC was able to account for 91% of the observed uncertainty.

The cumulative gas production in the repository due to corrosion and to microbial degradation can be combined to produce total gas production as shown in the left frame of Fig. 5. Most sample elements result in a total gas production over 10 000 yr between 5×10^8 and 1.2×10^9 mol. Also, most sample elements show a period of rapid gas production in the first few thousand years, with considerably reduced rates of gas production at later times. As shown in Fig. 6, the inventory of steel and cellulosics is often exhausted or significantly depleted after the first few thousand years.

The right frame in Fig. 5 presents sensitivity analysis results based on PRCCs for total gas production. Positive effects are indicated for GRCORH, GRMICH, STOICMIC and BRSAT, and negative effects are indicated for STOICCOR. For the entire

Fig. 4. Uncertainty and sensitivity analysis results for gas generation due to microbial degradation of cellulosics.

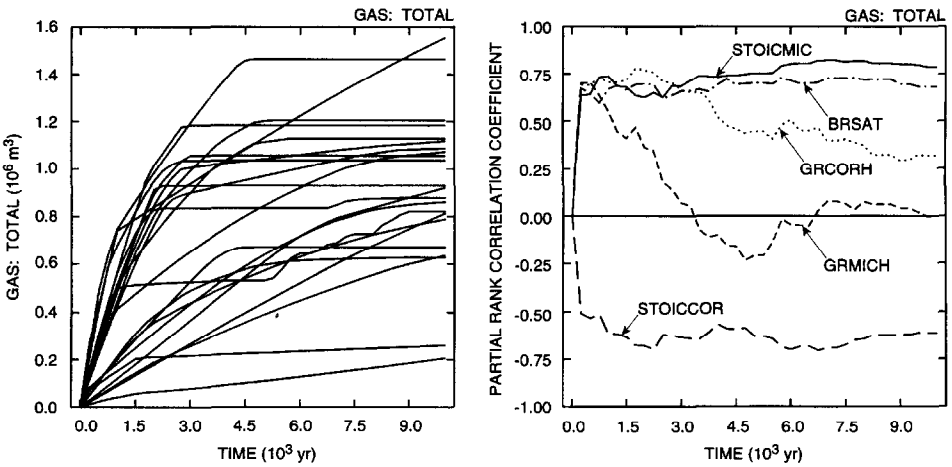

Fig. 5. Uncertainty and sensitivity analysis results for total gas production (i.e., both corrosion of steel and microbial degradation of cellulosics).

10 000 yr period, the most important variables are STOICMIC, BRSAT and STOICCOR.

The regression analysis for total gas production over 10 000 yr due to both corrosion and microbial degradation is presented at the bottom of Table 4. The only variable selected in the analysis is STOICMIC, which has a positive regression coefficient and can account for 33% of the uncertainty in total gas production. The indicated effect for STOICMIC is consistent with its dominant influence on gas generation due to microbial degradation as indicated in Fig. 4 and Table 4. However, a regression model with an R^2 value of 0.33 is failing to account for much of the uncertainty. As for cumulative gas production over 10 000 yr due to corrosion, the examination of scatter plots indicates that no single variable exerts a dominant influence on cumulative gas production due to corrosion and microbial degradation.

The two left frames in Fig. 6 show the time-dependent steel and cellulosic inventories associated with the individual sample elements. The two right frames present corresponding sensitivity analyses based on PRCCs. The steel inventory is initially dominated by VMETAL (fraction of total waste volume occupied by IDB metals and glass category), with the importance of this variable decreasing with time. The variables GRCORI, GRCORH and BRSAT have negative effects on the steel inventory. The negative relationships involving GRCORI, GRCORH and BRSAT result from their effects on increasing the rate of corrosion. The cellulosic inventory is initially dominated by VWOOD, with the importance of this variable decreasing rapidly with time. An additional positive effect is indicated for STOICMIC. Increasing STOICMIC tends to increase gas production and thus increase the fraction of the waste panel pore volume that is filled with gas; in turn, this reduces the rate at which cellulose is consumed by microbial degradation. Negative effects are indicated for GRMICI, GRMICH and BRSAT, with increasing values for each of these variables

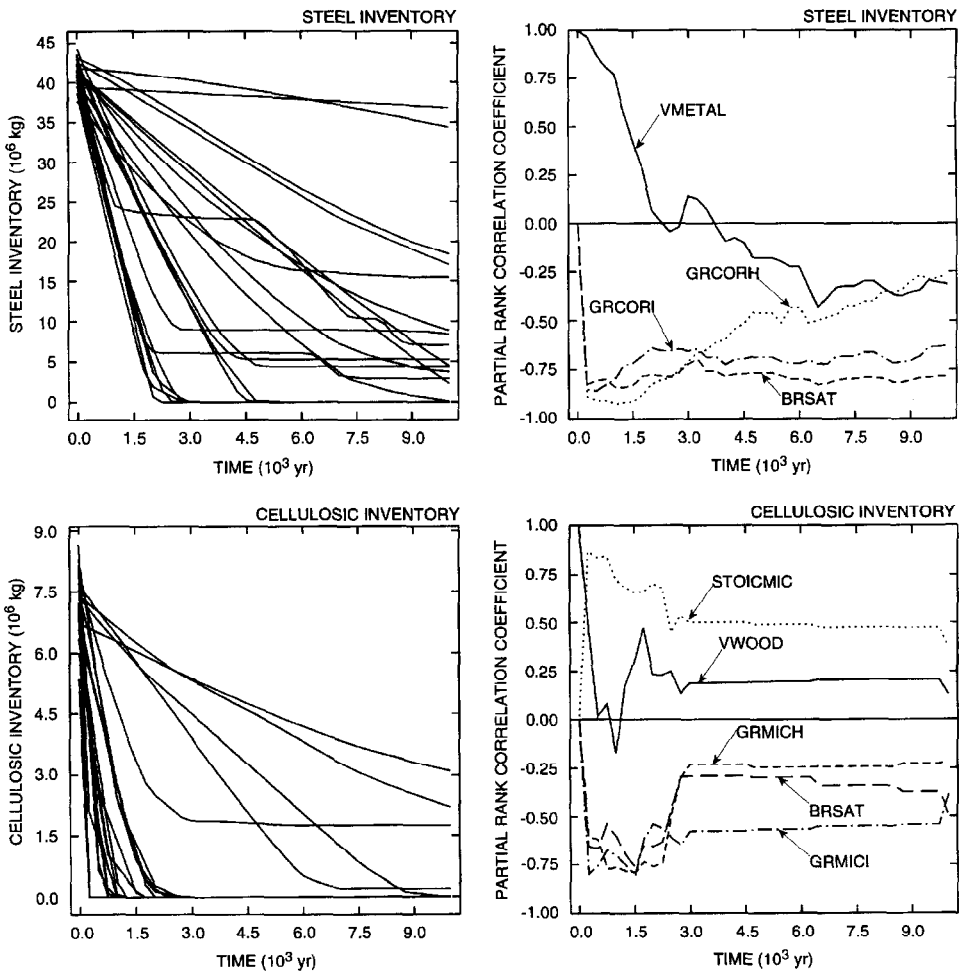

Fig. 6. Uncertainty and sensitivity analysis results for steel and cellulosic inventories in waste repository.

tending to increase the rate at which cellulose is consumed by microbial degradation. At times greater than 3000 yr, the cellulose inventory is completely depleted for most sample elements, with the result that the calculated partial correlation coefficients have little meaning due to the large number (i.e., 17 out of 22) of zeros involved.

5. Gas saturation and pressure in waste panel

Time-dependent values for average gas saturation in the individual waste blocks (i.e., averaged over entire waste block) are presented in the left column of Fig. 7.

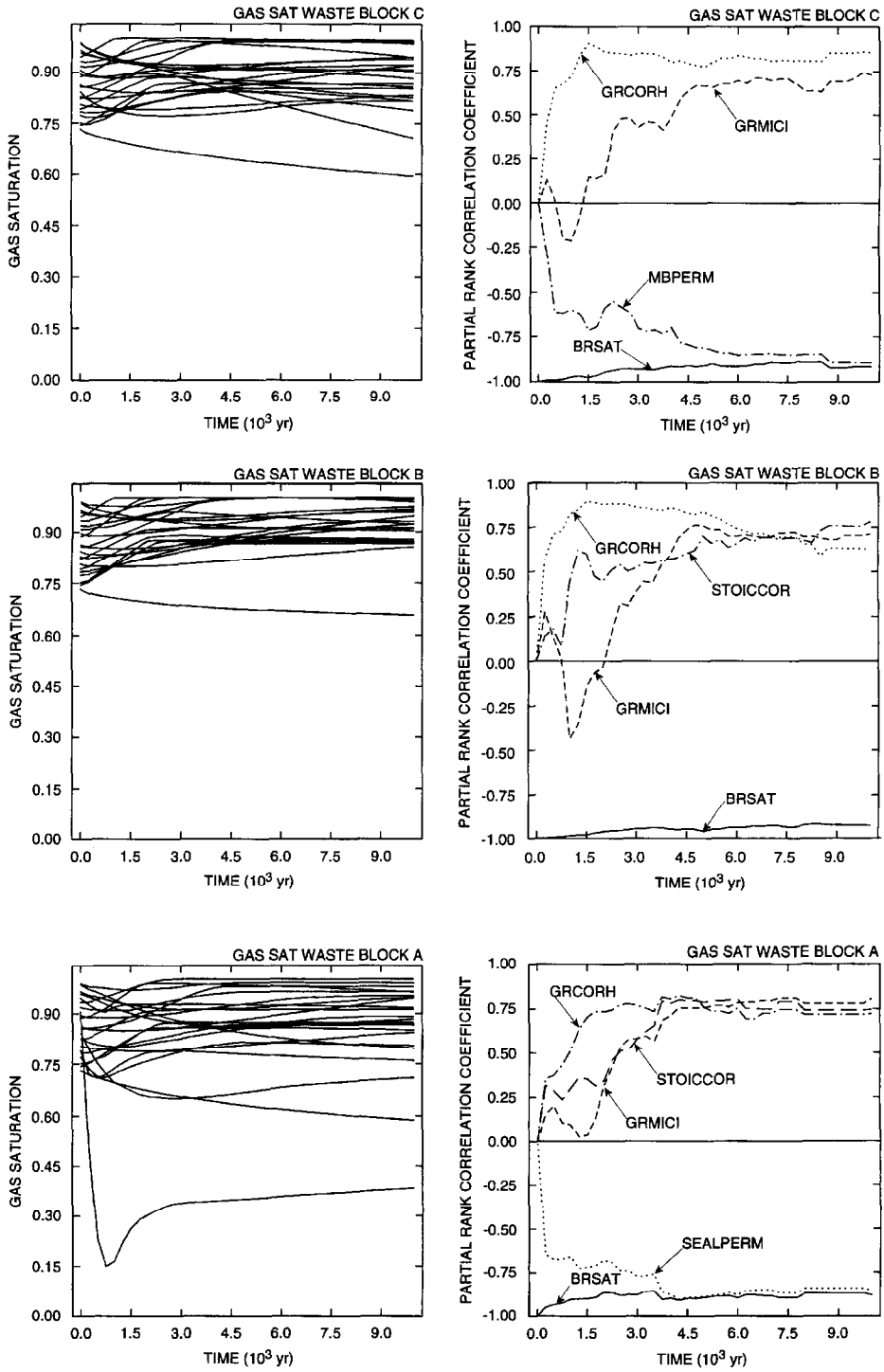

Fig. 7. Uncertainty and sensitivity analysis results for gas saturation in individual waste blocks.

Although gas saturation initially decreases for some sample elements, the overall tendency is for gas saturation to increase towards an asymptote with increasing time. The gas saturations in Waste Block A tend to be lower than those in Waste Blocks C and B. As shown in Fig. 1, Waste Block A is adjacent to the shaft and hence loses more gas by flow up the shaft than Waste Blocks C and B. As the PRCCs for gas saturation in the right column of Fig. 7 show for all three waste blocks, increasing GRCORH and GRMICI tends to increase gas saturation and increasing BRSAT tends to decrease gas saturation, with these effects resulting because increasing GRCORH and GRMICI increases the amount of gas in the panel and increasing BRSAT increases the amount of brine in the panel.

For Waste Block C, a negative effect is also indicated for MBPERM (marker bed permeability), with this effect occurring because increasing MBPERM increases the rate at which brine flows into Waste Block C from anhydrite layers in the Salado Formation. Due to the structure of the computational grid shown in Fig. 1, most inflowing brine enters the repository through Waste Block C. In addition, the variable STOICCOR appears in the analysis for gas saturation in Waste Block B. As discussed at the end of this section, increasing STOICCOR decreases the initial pore volume in the repository. Since the initial amount of brine is set as a fraction of the pore volume, increasing STOICCOR also reduces the amount of brine initially present in the pore space of the repository. Thus, as constant gas generation rates are assumed in this analysis, the total brine inventory can be depleted more rapidly when STOICCOR is large than when STOICCOR is small (i.e., because large values for STOICCOR result in less brine being initially present). This relationship between STOICCOR and amount of brine initially present in the repository is resulting in the positive correlations between STOICCOR and gas saturation in Waste Block B and also in Waste Block A. This relationship is an artifact of the manner in which initial repository pore volume was set in an attempt to incorporate the competing effects of gas generation and waste panel closure due to salt creep.

As shown in the left column of Fig. 8, time-dependent gas pressure in the individual waste blocks tends to increase monotonically until a maximum is reached and then undergoes a slower monotonic decrease. The largest gas pressures are approximately 2 MPa above the lithostatic pressure of 14.8 MPa. The gas pressures in the three waste blocks are quite similar. As comparison of the left column in Figs. 7 and 8 shows, there is more variability in gas saturation between the waste blocks than in gas pressure. Thus, gas appears to be flowing between the waste blocks to a greater extent than brine.

The PRCCs for gas pressure in the right column of Fig. 8 indicate that SEALPERM (permeability of seals between waste panels) and SH2PERM (middle shaft section permeability) are the two most important variables influencing gas pressure, with gas pressure tending to decrease as each of these variables increases. Prior to 5000 yr, gas pressure tends to increase as the variables GRCORH, GRMICH and BRSAT increase due to the influence of these variables on increasing gas production. However, as shown in Fig. 5, most gas production is over by 5000 yr, with the result that gas pressure is then controlled by variables such as SEALPERM and SH2PERM that influence gas flow out of the waste blocks.

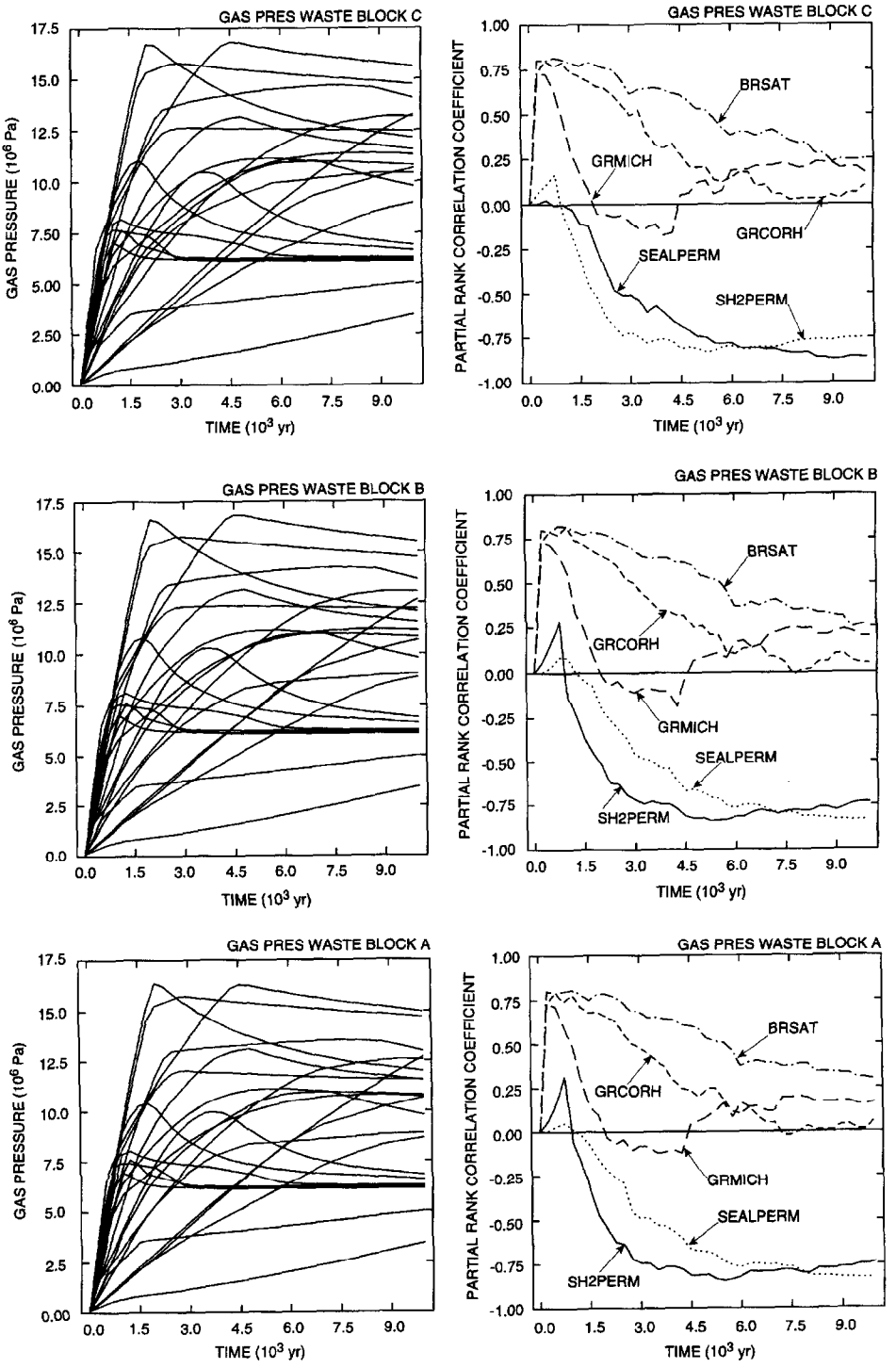

Fig. 8. Uncertainty and sensitivity analysis results for gas pressure in individual waste blocks.

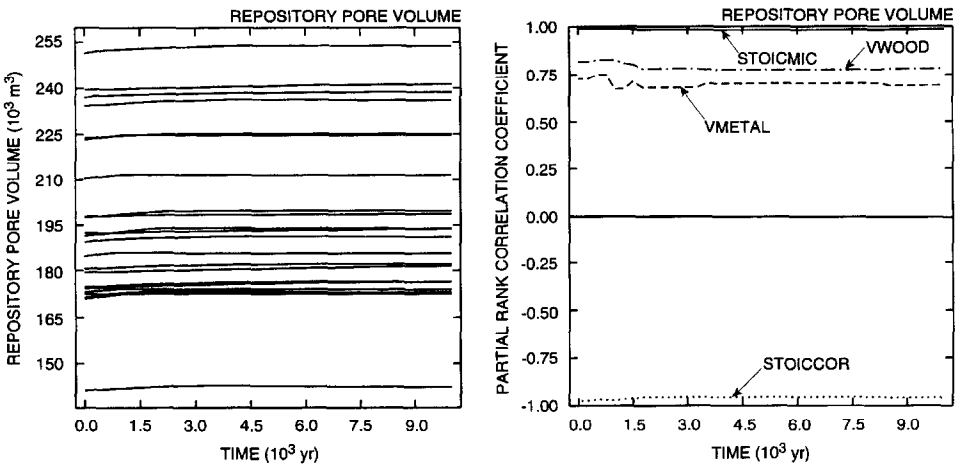

Fig. 9. Uncertainty and sensitivity analysis results for total pore volume in repository.

The 1991 WIPP PA did not directly model closure of the waste panels. Instead, the interaction of gas generation and panel closure was incorporated into the analysis by setting the initial pore volume in each waste panel to the volume necessary to contain all waste-generated gas at lithostatic pressure (i.e., 14.8 MPa) as described in Section 3.1 of Ref. [16]. As a result, initial pore volume is a function of STOICCOR, STOICMIC, VMETAL and VWOOD. As shown in the left frame of Fig. 9, pore volume remains essentially fixed at its initial volume, although there is a small response to changing gas pressures through rock compressibility effects. Further, the PRCCs in the right frame of Fig. 9 indicate that pore volume is indeed a function of STOICCOR, STOICMIC, VMETAL and VWOOD.

6. Gas migration

A primary focus of this study and its two companion studies [21, 22] is the migration of gas away from the waste panels. For this presentation, this means gas migration through the shaft to the Culebra Dolomite. As shown by the two left frames in Fig. 10, most gas leaving the repository flows up the shaft to the Culebra Dolomite.

Sensitivity analysis results based on PRCCs for cumulative gas flow out of the repository are given in the upper right frame of Fig. 10. These results indicate that total gas flow out of the repository tends to increase with increasing gas generation and decreasing resistance to gas flow. In particular, gas outflow increases as BRSAT, GRCORI and GRCORH increase due to the effect of these variables on increasing gas generation, and gas outflow increases as SEALPERM and SH2PERM increase due to decreased resistance to gas flow.

The sensitivity analysis results for cumulative gas flow through the shaft to the Culebra Dolomite appear in the lower right of Fig. 10. As examination of the PRCCs

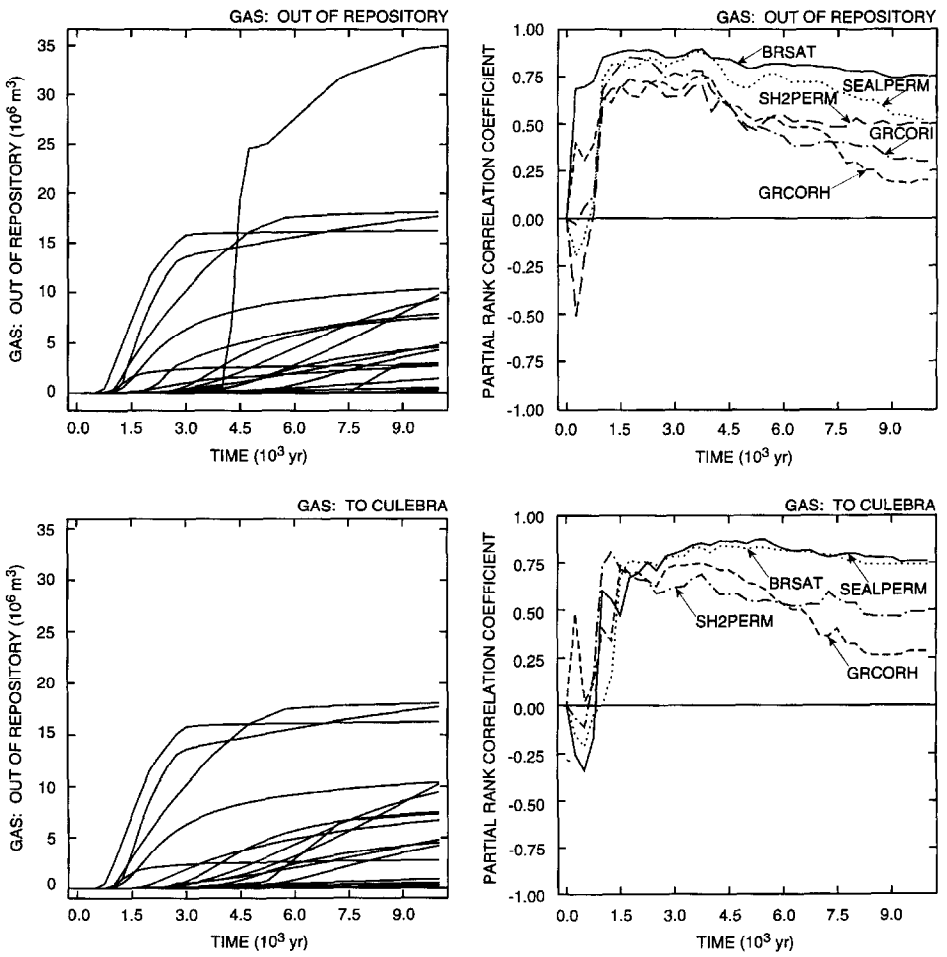

Fig. 10. Uncertainty and sensitivity analysis results for cumulative gas flow out of repository and through shaft to Culebra Dolomite.

in this frame shows, the analysis is initially unstable with wide swings in the values for these coefficients. This instability results from the fact that many of the releases to the Culebra Dolomite are 0 at early times (i.e., <1500 yr), with the result that the analysis results are dominated by random noise for the first 1500 yr (e.g., changing from 19 zeros out of 22 observations to 18 zeros out of 22 observations can cause large, but meaningless, swings in the values for the partial correlation coefficients). After about 3000 yr, the effects of the individual variables are clearer, with positive effects indicated for variables that increase gas generation (i.e., BRSAT and GRCORH) and decrease resistance to gas flow (i.e., SEALPERM and SH2PERM). However, four sample elements result in no release to the Culebra, which tends to reduce the effectiveness of the PRCCs in identifying the effects of individual variables.

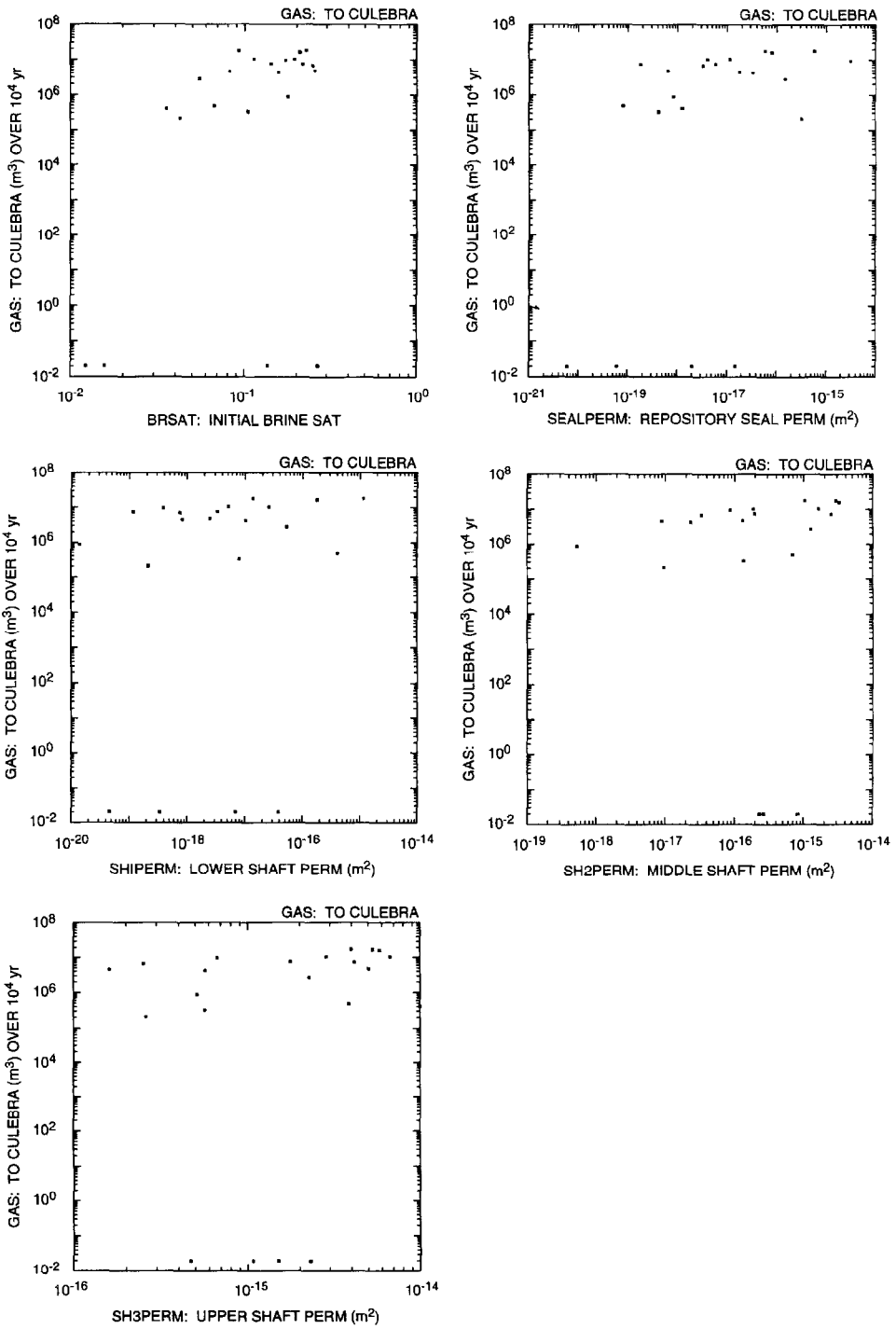

Fig. 11. Scatter plots for cumulative gas flow over 10 000 yr through the shaft to the Culebra Dolomite for following variables: BRSAT, SEALPERM, SH1PERM, SH2PERM and SH3PERM.

When zero observations and possibly other patterns of behavior are present, the examination of scatter plots can help reveal the relationships between sampled and calculated variables. The scatter plots for cumulative gas flow through the shaft to the Culebra Dolomite over 10 000 yr versus five individual variables are shown in Fig. 11. These variables were selected as having the strongest relationships with cumulative gas flow through the shaft to the Culebra Dolomite on the basis of a visual examination of the scatter plots for the 16 variables defined in Table 2. Although all the scatter plots show a positive relationship between the sampled variable and cumulative gas flow, none of the relationships are very tight. Further, the four zero releases are scattered over the range of each sampled variable. Thus, no single variable appears to dominate cumulative gas release to the Culebra. As shown in Eq. (13), the shaft seal permeabilities SH1PERM, SH2PERM and SH3PERM are correlated, and only the middle shaft permeability SH2PERM was included in the partial correlation analysis.

Very little brine migration away from the waste panels occurred. Of the 22 sample elements used in this analysis, only 4 resulted in brine migration away from the waste panels.

7. Discussion

The inventories of steel and cellulosics are substantially consumed by corrosion and microbial degradation for most sample elements. Variables affecting gas generation rates are important for gas production at early times but not for gas production over the entire 10 000 yr period under consideration. Overall, the most important variables for total gas production are the two stoichiometric terms and initial brine saturation.

The analyses often produce brine saturations that are below residual brine saturation when averaged over entire waste blocks. Thus, there are significant regions within the individual waste panels in which brine flow will not take place. Under such conditions, radionuclides cannot be transported from these regions by flowing brine.

Pressures in the waste blocks typically remained below lithostatic pressure (i.e., 14.8 MPa). However, this may be primarily due to an analysis assumption made to resolve the competing effects of gas pressurization of the waste panels and compaction of the waste due to overburden pressure.

Gas flow to the Culebra resulted for 18 of the 22 sample elements used in the analysis. Thus, the sealing system modeled in this analysis does not prevent gas flow to the Culebra. The dominant variables with respect to such flow were initial brine saturation in the waste, permeability of seals between waste blocks, and permeability of seals in the shaft. In contrast, brine flows away from the waste panels occurred for only 4 of the 22 sample elements. The importance of panel seal permeability results in part from the assumption that the disturbed rock zone permeability is sufficiently low to prevent significant quantities of gas from bypassing the panel seals.

The present analysis used a Latin hypercube sample of size 22 from 16 imprecisely known variables. Comparison of analysis results with those obtained in Ref. [21], which used a sample of size 60 from 14 variables, suggests that use of a somewhat

larger sample size would have produced better-defined results. However, it is unlikely that any of the insights obtained in the analysis would change significantly.

The uncertainty and sensitivity analysis techniques used in this study provide a powerful technique for model verification. Reassuringly, no errors in the implementation or operation of BRAGFLO were observed.

Acknowledgements

The support provided by D.R. Anderson, B.L. Baker, J. Berglund, W. Beyeler, S.C. Hora, H.J. Iuzzolino, R.P. Rechard, D.K. Rudeen, M.S. Tierney, K. Trauth and other members of the 1991 WIPP PA team is gratefully acknowledged. Special recognition is extended to M.G. Marietta and M. Fewell for their careful prepublication review of this document. The editorial support provided by the staff of Tech Reps, Inc., with special thanks to D. Sessions, J. Ripple and H. Olmstead, is also gratefully appreciated. Work performed for Sandia National Laboratories and the US Department of Energy under contract DE-AC04-76-DP00789.

References

[1] US DOE (Department of Energy), Final Environmental Impact Statement: Waste Isolation Pilot Plant, DOE/EIS-0026, Vols. 1–2, U.S. Department of Energy, Washington, DC, 1980.

[2] US DOE (Department of Energy), Final Supplement Environmental Impact Statement, Waste Isolation Pilot Plant, DOE/EIS-0026-FS, Vols. 1–13, US Department of Energy, Office of Environmental Restoration and Waste Management, Washington, DC, 1990.

[3] US DOE (Department of Energy), Strategy for the Waste Isolation Pilot Plant Test Phase, Revised Draft #3, DOE/EM/48063-2, US Department of Energy, Office of Waste Operations, Washington, DC, 1991.

[4] US EPA (Environmental Protection Agency), Land Disposal Restrictions, Code of Federal Regulations 40, Part 268, Office of the Federal Register, National Archives and Records Administration, Washington, DC, 1986.

[5] US EPA (Environmental Protection Agency), Environmental Standards for the Management and Disposal of Spent Nuclear Fuel, High-Level and Transuranic Radioactive Wastes; Final Rule, 40 CFR Part 191, Federal Register 50 (1985) 38 066–38 089.

[6] S.G. Bertram-Howery and R.L. Hunter (Eds.), Preliminary Plan for Disposal-System Characterization and Long-Term Performance Evaluation of the Waste Isolation Pilot Plant, SAND89-0178, Sandia National Laboratories, Albuquerque, NM, 1989.

[7] A.R. Lappin, R.L. Hunter, D.P. Garber, P.B. Davies, R.L. Beauheim, D.J. Borns, L.H. Brush, B.M. Butcher, T. Cauffman, M.S.Y. Chu, L.S. Gomez, R.V. Guzowski, H.J. Iuzzolino, V. Kelley, S.J. Lambert, M.G. Marietta, J.W. Mercer, E.J. Nowak, J. Pickens, R.P. Rechard, M. Reeves, K.L. Robinson and M.D. Siegel, Systems Analysis, Long-Term Radionuclide Transport, and Dose Assessments, Waste Isolation Pilot Plant (WIPP), Southeastern New Mexico; March 1989, SAND89-0462, Sandia National Laboratories, Albuquerque, NM, 1989.

[8] M.G. Marietta, S.G. Bertram-Howery, D.R. Anderson, K.F. Brinster, R.V. Guzowski, H. Iuzzolino and R.P. Rechard, Performance Assessment Methodology Demonstration: Methodology Development for Evaluating Compliance with EPA 40 CFR 191, Subpart B, for the Waste Isolation Pilot Plant, SAND89-2027, Sandia National Laboratories, Albuquerque, NM, 1989.

[9] S.G. Bertram-Howery, M.G. Marietta, R.P. Rechard, P.N. Swift, D.R. Anderson, B.L. Baker, J.E. Bean, Jr., W. Beyeler, K.F. Brinster, R.V. Guzowski, J.C. Helton, R.D. McCurley, D.K. Rudeen,

J.D. Schreiber and P. Vaughn, Preliminary Comparison with 40 CFR Part 191, Subpart B for the Waste Isolation Pilot Plant, December 1990, SAND90-2347, Sandia National Laboratories, Albuquerque, NM, 1990.

[10] WIPP PA (Performance Assessment) Division, Preliminary Comparison with 40 CFR Part 191, Subpart B for the Waste Isolation Pilot Plant, December 1991, Vol. 1: Methodology and Results, SAND91-0893/1, Sandia National Laboratories, Albuquerque, NM, 1991.

[11] WIPP PA (Performance Assessment) Department, Preliminary Performance Assessment for the Waste Isolation Pilot Plant, December 1992 – Vol. 1: Third Comparison with 40 CFR 191, Subpart B. SAND92-0700/1, Sandia National Laboratories, Albuquerque, NM, 1992.

[12] WIPP PA (Performance Assessment) Division, Preliminary Comparison with 40 CFR Part 191, Subpart B for the Waste Isolation Pilot Plant, December 1991, Vol. 2: Probability and Consequence Modeling, SAND91-0893/2, Sandia National Laboratories, Albuquerque, NM, 1991.

[13] WIPP PA (Performance Assessment) Division, Preliminary Comparison with 40 CFR Part 191, Subpart B for the Waste Isolation Pilot Plant, December 1991, Vol. 3: Reference Data, SAND91-0893/3, Sandia National Laboratories, Albuquerque, NM, 1991.

[14] J.C. Helton, J.W. Garner, R.P. Rechard, D.K. Rudeen and P.N. Swift, Preliminary Comparison with 40 CFR Part 191, Subpart B for the Waste Isolation Pilot Plant, December 1991, Vol. 4: Uncertainty and Sensitivity Analysis Results, SAND91-0893/4, Sandia National Laboratories, Albuquerque, NM, 1992.

[15] J.C. Helton, J.W. Garner, M.G. Marietta, R.P. Rechard, D.K. Rudeen and P.N. Swift, Nucl. Sci. Eng., 114 (1993) 286.

[16] J.C. Helton, D.R. Anderson, B.L. Baker, J.E. Bean, J.W. Berglund, W. Beyeler, J.W. Garner, H.J. Iuzzolino, M.G. Marietta, R.P. Rechard, P.J. Roache, D.K. Rudeen, J.D. Schreiber, P.N. Swift, M.S. Tierney and P. Vaughn, Nucl. Eng. Des., 154 (1995) 251.

[17] WIPP PA (Performance Assessment) Department, Long-Term Gas and Brine Migration at the Waste Isolation Pilot Plant: Preliminary Sensitivity Analyses for Post-Closure 40 CFR 268 (RCRA), May 1992, SAND92-1933, Sandia National Laboratories, Albuquerque, NM, 1992.

[18] J.C. Helton, J.E. Bean, B.M. Butcher, J.W. Garner, J.D. Schreiber, P.N. Swift and P. Vaughn, Uncertainty and Sensitivity Analyses for Gas and Brine Migration at the Waste Isolation Pilot Plant, May 1992, SAND92-2013, Sandia National Laboratories, Albuquerque, NM, 1993.

[19] J.C. Helton, J.W. Garner, R.D. McCurley and D.K. Rudeen, Sensitivity Analysis Techniques and Results for Performance Assessment at the Waste Isolation Pilot Plan, SAND90-7103, Sandia National Laboratories, Albuquerque, NM, 1991.

[20] J.C. Helton, Reliab. Eng. System Safety, 42 (1993) 327.

[21] J.C. Helton, J.E. Bean, B.M. Butcher, J.W. Garner, J.D. Schreiber, P.N. Swift and P. Vaughn, Nucl. Sci. Eng., in press.

[22] J.C. Helton, J.E. Bean, B.M. Butcher, J.W. Garner, J.D. Schreiber, P.N. Swift and P. Vaughn, in preparation.

[23] Bechtel, Inc., Design Validation Final Report, DOE/WIPP-86-010, Prepared for US Department of Energy, Bechtel National, Inc., San Francisco, CA, 1986.

[24] E.J. Nowak, J.R. Tillerson and T.M. Torres, Initial Reference Seal System Design: Waste Isolation Pilot Plant, SAND90-0355, Sandia National Laboratories, Albuquerque, NM, 1990.

[25] C.I. Voss, SUTRA (Saturated-Unsaturated Transport): A Finite-Element Simulation Model for Saturated-Unsaturated, Fluid-Density-Dependent Ground-Water Flow with Energy Transport or Chemically-Reactive Single-Species Solute Transport, Water-Resources Investigations Report 84-4369, US Geological Survey National Center, Reston, VA, 1974.

[26] H.B. Crichlow, Modern Reservoir Engineering – A Simulation Approach, Prentice-Hall, Englewood Cliffs, NJ, 1977.

[27] D.W. Peaceman, Fundamentals of Numerical Reservoir Simulation: Developments in Petroleum Science 6, Elsevier, New York, 1977.

[28] P.B. Davies, Evaluation of the Role of Threshold Pressure in Controlling Flow of Waste-Generated Gas into Bedded Salt at the Waste Isolation Pilot Plant, SAND90-3246, Sandia National Laboratories, Albuquerque, NM, 1991.

[29] M.A. Molecke, Gas Generation from Transuranic Waste Degradation: Data Summary and Interpretation, SAND79-1245, Sandia National Laboratories, Albuquerque, NM, 1979.
[30] Oak Ridge National Laboratory, 1990 Integrated Data Base: Spent Fuel and Radioactive Waste Inventories, Projection and Characteristics, DOE/RW-0006, Rev. 6, Oak Ridge National Laboratory, Oak Ridge, TN, 1990.
[31] J.C. Helton, Nucl. Technol., 101 (1993) 18.
[32] J.C. Helton, Risk Anal., 14 (1994) 483.
[33] M.D. McKay, R.J. Beckman and W.J. Conover, Technometrics 21 (1979) 239–245.
[34] R.L. Iman and M.J. Shortencarier, A FORTRAN 77 Program and User's Guide for the Generation of Latin Hypercube and Random Samples for Use with Computer Models, NUREG/CR-3624, SAND83-2365, Sandia National Laboratories, Albuquerque, NM, 1984.
[35] R.L. Iman and W.J. Conover, Commun. Statist. Simulation Comput., 11 (1982) 311.
[36] W.H. Beyer (Ed), CRC Handbook of Tables for Probability and Statistics, Chemical Rubber Co, Cleveland, OH, 2nd edn., 1968.
[37] F.N. David, Tables of the Ordinates and Probability Integral of the Distribution of the Correlation Coefficient in Small Samples, Biometrika Office, University College London; Cambridge, The University Press, Cambridge, 1938.
[38] R.L. Iman, M.J. Shortencarier and J.D. Johnson, A FORTRAN 77 Program and User's Guide for the Calculation of Partial Correlation and Standardized Regression Coefficients, NUREG/CR-4122, SAND85-0044, Sandia National Laboratories, Albuquerque, NM, 1985.
[39] R.L. Iman and W.J. Conover, Technometrics, 21 (1979) 499.
[40] R.L. Iman, J.M. Davenport, E.L. Frost and M.J. Shortencarier, Stepwise Regression with PRESS and Rank Regression (Program User's Guide), SAND79-1472, Sandia National Laboratories, Albuquerque, NM, 1980.
[41] N.R. Draper and H. Smith, Applied Regression Analysis, Wiley, New York, 2nd edn., 1981.
[42] D.M. Allen, The Prediction Sum of Squares as a Criterion for Selecting Predictor Variables Report No. 23, Department of Statistics, University of Kentucky, Lexington, KY, 1971.